Photosynth Res
DOI 10.1007/s11120-015-0148-3

REGULAR PAPER

Electronic coupling of the phycobilisome with the orange carotenoid protein and fluorescence quenching

Igor N. Stadnichuk[1] · Pavel M. Krasilnikov[2] · Dmitry V. Zlenko[2] · Alexandra Ya. Freidzon[3] · Mikhail F. Yanyushin[4] · Andrei B. Rubin[2]

Received: 18 December 2014 / Accepted: 18 April 2015

Abstract Using computational modeling and known 3D structure of proteins, we arrived at a rational spatial model of the orange carotenoid protein (OCP) and phycobilisome (PBS) interaction in the non-photochemical fluorescence quenching. The site of interaction is formed by the central cavity of the OCP monomer in the capacity of a keyhole to the characteristic external tip of the phycobilin-containing domain (PB) and folded loop of the core-membrane linker L_{CM} within the PBS core. The same central protein cavity was shown to be also the site of the OCP and fluorescence recovery protein (FRP) interaction. The revealed geometry of the OCP to the PBL_{CM} attachment is believed to be the most advantageous one as the L_{CM}, being the major terminal PBS fluorescence emitter, gathers, before quenching by OCP, the energy from most other phycobilin chromophores of the PBS. The distance between centers of mass of the OCP carotenoid 3′-hydroxyechinenone (hECN) and the adjacent phycobilin chromophore of the PBL_{CM} was determined to be 24.7 Å. Under the dipole–dipole approximation, from the point of view of the determined mutual orientation and the values of the transition dipole moments and spectral characteristics of interacting chromophores, the time of the direct energy transfer from the phycobilin of PBL_{CM} to the S_1 excited state of hECN was semiempirically calculated to be 36 ps, which corresponds to the known experimental data and implies the OCP is a very efficient energy quencher. The complete scheme of OCP and PBS interaction that includes participation of the FRP is proposed.

Keywords Allophycocyanin · Fluorescence · L_{CM}–polypeptide · Orange carotenoid protein · Phycobilisome(s) · Quenching

Abbreviations

APC	Allophycocyanin
EET	Electronic energy transfer
hECN	3′-hydroxyechinenone
ICT	Internal charge transfer
FRP	Fluorescence recovery protein
L_{CM}	Long-wavelength terminal emitter
NPQ	Non-photochemical fluorescence quenching
OCP	Orange carotenoid protein
PBL_{CM}	Phycobilin-containing domain of L_{CM}
PBS	Phycobilisome

✉ Dmitry V. Zlenko
dvzlenko@gmail.com

[1] K. A. Timiryazev Institute of Plant Physiology RAS, Botanicheskaya, 35, 127726 Moscow, Russia

[2] Biological Faculty of Lomonosov Moscow State University, Lenin Hills, 119991 Moscow, Russia

[3] Photochemical Centre of Russian Academy of Sciences, Novatorov, 7a/1, 119071 Moscow, Russia

[4] Institute of Fundamental Problems of Biology, Russian Academy of Sciences, Institutskaya, 2, 142290 Pushchino, Moscow Region, Russia

Introduction

The primary light-harvesting antennae in cyanobacteria are phycobilisomes (PBSs), giant complexes of phycobiliproteins connected by linker polypeptides and containing covalently bound phycobilin pigments. Hemi-discoidal PBSs, the most common type, consist of (i) a central tricylindrical core composed of disk-shaped allophycocyanin (APC)

Published online: 07 May 2015

trimers and (ii) six lateral tube-like rods emanating fanlike from the core and built up of stacked hexamers of other phycobiliproteins (Adir 2005; Watanabe and Ikeuchi 2013). The short-term light-adaptation process that reversibly increases thermal dissipation of excess energy in PBS (Rakhimberdieva et al. 2004; Wilson et al. 2006) is called non-photochemical fluorescence quenching (NPQ). This harmless photoprotective mechanism, which decreases the amount of energy arriving from PBSs at the photosystem II and photosystem I reaction centers (Rakhimberdieva et al. 2001; Mullineaux 2008), and is observed as well in the ancient thylakoid-less cyanobacterium *Gloeobacter violaceus*, is evolutionarily rather old (Bernát et al. 2011).

The water-soluble orange carotenoid protein (OCP) contains a single noncovalently bound molecule of the ketocarotenoid 3′-hydroxyechinenone (hECN) (Holt and Krogmann 1981) and is known to realize NPQ, diminishing the effectiveness of PBS light harvesting, although the structural details of this process have not been well elucidated (Kirilovsky and Kerfeld 2013). The OCP exists in two distinct conformational states: an inactive, dark-stable orange form (OCP^o) and a photoactive, metastable red form (OCP^r) that can be generated by intense blue–green light and causes photoprotection (Wilson et al. 2008). OCP deactivates the excited state of PBS rather effectively: approximately 30–40 % of the absorbed light energy in the wild type cells of *Synechocystis* sp. PCC6803 (hereafter referred to as *Synechocystis*) can be thermally dissipated upon OCP light-dependent induction (Wilson et al. 2008; Rakhimberdieva et al. 2010). The OCP acts as a photosensor and also as an effector with direct contact with PBS (Stadnichuk et al. 2011b; Gwizdala et al. 2011). The structural location of the OCP^r during the time of contact with the PBS is extremely important to evaluation of the molecular quenching mechanism. The large—two orders of magnitude (35 vs. ~3000–5000 kDa)—difference between the molecular masses of OCP and PBS, respectively (Holt and Krogmann 1981; Adir 2005; Watanabe and Ikeuchi 2013) and the small (≤0.5) OCP to PBSs ratio in the cell (Gwizdala et al. 2011) means that the structural location of the OCP when it is bound to the PBS has to be very specific. As *Synechocystis* cyanobacterial mutants lacking lateral PBS cylinders were still capable of OCP-induced quenching, the OCP^r binding site was attributed to the PBS core by different groups and laboratories (Scott et al. 2006; Wilson et al. 2008; Stadnichuk et al. 2009). The tricylindrical core subcomplex (M ~ 1.200 kDa) consists of one upper and two having contact with the thylakoid membrane basal cylinders; each of these is composed of four stacked $(\alpha\beta)_3$-APC trimers (Adir 2005; Watanabe and Ikeuchi 2013). The phycocyanobilin chromophores covalently bound to cysteine residues α84 and β84 are packed rigidly in their respective pigment-binding pockets. The PBS core also possesses in both basal cylinders three less abundant solely chromophorylated red-shifted polypeptides: ApcD (α-subunit of allophycocyanin B, or α^B), ApcF (β^{18} polypeptide), and L_{CM} (=ApcE, or anchor protein) (Adir 2005; Watanabe and Ikeuchi 2013). Together with bulk APC and a small colorless linker, $L_{7.8}$, these subunits form four kinds of APC trimers: $(\alpha\beta)_3$, $(\alpha\beta)_3L_{7.8}$, $(\alpha\beta)_2(\alpha^B\beta)$, and $(\alpha\beta)_2(PBL_{CM}\beta^{18})$, where PBL_{CM} indicates the homologous to the αAPC chromophorylated domain of 90 kDa L_{CM}. In accordance with their role of long-wavelength terminal PBS emitters, the chromophorylated subunits replace corresponding α- and β-polypeptides of APC and mediate the excitation energy transfer from PBS core to the photosynthetic reaction centers (Adir 2005; Watanabe and Ikeuchi 2013). Unlike ApcD and ApcF (Jallet et al. 2012; Stadnichuk et al. 2012), the established interaction of OCP with purified L_{CM} in vitro (Stadnichuk et al. 2012) completed with the data of various spectral and biochemical experiments in vivo and examination of an L_{CM}-less *Synechocystis* mutant (Stadnichuk et al. 2013) indicated that OCP most probably quenches the PBL_{CM}-chromophore, and this event might have a crucial role in the NPQ of cyanobacteria. It was concluded that besides being a very central element in PBS to reaction center excitation energy transfer and PBS assembly, L_{CM} also has an essential role in the photoprotective light-adaptation processes of cyanobacteria (Stadnichuk et al. 2013). Because PBL_{CM} accumulates energy from most of the dozens of short-wavelength chromophores of the PBS (Adir 2005; Watanabe and Ikeuchi 2013), it is likely that only one single hECN-phycobilin quenching pair out of all presumably available PBS phycobilins could suffice as a quenching center.

There are no structural (crystallographic or NMR) data for the PBS protein architectural ensemble, OCP^r, and L_{CM}. Nevertheless, comparison of the single particle electron microscopy images (13 Å resolution) of PBS core (Arteni et al. 2009) and the resolved structures of APC crystals are convinced of their high similarity. As for OCP, recently it was shown that the main event in OCP^o to OCP^r photoconversion in cyanobacterial cell is the monomerization of OCP^o dimers while the simultaneously registered absorption spectrum changes of hECN accompany this process (Zhang et al. 2014). It makes the forcible argument for determining the most probable spatial arrangement of the OCP–PBS complex in silico by computational modeling (Stadnichuk et al. 2013; Zhang et al. 2014) based on the crystal structures of OCP^o (Kerfeld 2004) and APC (Brejc et al. 1995). The OCP is composed of two nearly equal *N*- and *C*-terminal domains separated by a central cavity; the carotenoid spans both domains (Kerfeld 2004; Wilson et al. 2010). The total cavity-volume equal to 895 $Å^3$ was

proposed large enough for a substantial interaction with another protein (Kerfeld 2004). Using a docking procedure and known 3D structure of proteins, it turned out that the characteristic tip on the lateral surface of the APC trimer and the interdomain cavity of the OCP molecule form the model of the probable site of the OCP and PBS interaction (Stadnichuk et al. 2013). In the present work, using molecular dynamics (MD) simulations and estimation of the free energy of the protein–protein structural interactions between the OCP and APC, we confirm the thermodynamic possibility of the recently obtained 3D model (Stadnichuk et al. 2013). We also demonstrate that the chromophorylated 25 kDa PBL_{CM}-domain, being geometrically similar to the αAPC (McGregor et al. 2008; Gao et al. 2012), could substitute for it in an APC trimer using molecular modeling methods. Applying the obtained 3D form of the PBL_{CM} that includes the folded PB loop, we arrived at a rational spatial model of the OCP to the PBS attachment. The thus developed 3D construction of the OCP–$(\alpha\beta)_2(PBL_{CM}\beta^{18})$ supercomplex fully corresponds to the high-affinity interaction of the OCP and PBS through the established biochemical instrumentality of OCP and L_{CM} (Stadnichuk et al. 2012, 2013). The final optimized geometrical model is evaluated to be reasonable without a steric clash.

The molecular mechanism of the OCP-induced NPQ in cyanobacteria is an active area of research. As pointed out (Tian et al. 2012), it is obvious that the process of quenching is the same in vitro and in vivo, but it is not fully understood, this being an open question. The difficult task of the determining the mechanism is the lack of structural data. From presented model, it is possible to imagine how the carotenoid of the OCP concealed by amino acids could interact with the nearest phycobilin chromophore of PBL_{CM} to quench the energy absorbed by the PBS. The model reveals a large surface contact between PBS and the OCP and determines the inter-chromophore distance of about 25 Å between the hECN and neighboring phycobilin molecule. Another one problem of evaluating the NPQ-mechanism is due to the complex spectral properties of carotenoids. In recent years, the photophysics of carotenoids has become better understood (Polívka and Sundström 2004). Recent data on the forbidden for absorption S_1 energy level of the OCP-carotenoid hECN in its photoactive and photoinactive states (Polívka et al. 2013) might facilitate the determination of the exact molecular mechanism of the blue–green light-induced NPQ in cyanobacteria. We demonstrate that the use of the constructed 3D model of OCP binding to the PBS core elucidates the underlying physical mechanism of quenching. From the point of view of the revealed mutual orientation and the values of the transition dipole moments and spectral characteristics of interacting chromophores, the results of our quantum chemical calculations give evidence for excitonic coupling of PBL_{CM}–phycobilin and the hECN chromophores during the process of quenching and dissipation of the light energy absorbed by PBSs. The time of the direct energy transfer from the excited phycobilin molecule of PBL_{CM} to the S_1 excited state of hECN was semiempirically calculated to be 36 ps, which corresponds to the known experimental data and implies the OCP is a very efficient energy quencher.

Except the OCP, process of PBS quenching in a cyanobacterial cell includes participation of the fluorescence recovery protein (FRP) (Boulay et al. 2010). It is a relatively small 13 kDa chromophore-less protein on the operon with the OCP that accelerates the reversibility of the NPQ process and thus restores the PBS fluorescence in the dark (Boulay et al. 2010; Sutter et al. 2013). Like PBS, the FRP interacts with the red active form of OCP (Gwizdala et al. 2013). We applied the crystal data of the FRP structure (Sutter et al. 2013) to a docking procedure to compare the sites of OCP/PBS and OCP/FRP attachment. In agreement with the particular role of the OCP intradomain cavity and FRP functionality, we demonstrate that FRP could be wedged in the OCP cavity weakening the PBS and OCP interaction. Therefore, a complete scheme of the interaction of OCP and the PBS that includes participation of FRP during quenching is proposed.

Materials and methods

Culture conditions

Synechocystis sp. PCC 6803 wild type and the CK mutant (Δ*cpc* operon) lacking lateral rods and preserving the APC core of PBSs (Ajlani et al. 1995) were routinely grown for 3–5 days at 30 °C with constant shaking in liquid BG-11 medium with twice the concentration of sodium nitrate, in continuous white fluorescent light of 40 μmol photons $m^{-2}s^{-1}$. The CK mutant was maintained in the presence of the appropriate antibiotics. Before phycobilisomes isolation procedures, the cyanobacterial cells were harvested by centrifugation and washed twice in 0.8 M phosphate buffer, pH 7.0.

Isolation procedures

Isolation of PBS

PBSs from the CK mutant were isolated according to the method of Glazer (1988). After harvesting, the *Synechocystis* cells were disrupted using a French press at 20,000 p.s.i. and purified by 0.25–0.80 sucrose density gradient ultracentrifugation. The fraction of intact PBSs, which formed the lower narrow blue band in the gradient, was collected in 0.8 M phosphate buffer at pH 7.0.

Purification of APC

APC was isolated from broken CK mutant cells (see "Isolation of PBS" section) on a Whatman DE-52 cellulose column, pre-purified on hydroxyapatite Bio-Gel HT (BioRad), and purified on DEAE Fractogel TSK 650 M (Merck) according to chromatographic method used to avoid contaminations of low molecular weight colorless linker and minor chromophorylated polypeptides of PBS core as described in detail in (Gottschalk et al. 2008). The absorption ratio $A_{652}/A_{275} \geq 1.8$ was used as acceptable purity.

Purification of OCP

OCP was isolated from disrupted *Synechocystis* cells (see "Isolation of PBS" section) by hydrophobic interaction chromatography using a reverse gradient of ammonium sulfate on butyl-TSK followed by ion-exchange chromatography on a TSK-DEAE column as described previously (Stadnichuk et al. 2013). The absorption ratio of A_{465}/A_{275} above 1.9 was used for acceptable purity. OCP fraction was stored in 5 mM Tris–HCl, 80 mM NaCl (pH 8.0) at −70 °C prior to use.

Extraction of hECN

The noncovalently bound carotenoid, hECN, was extracted by incubating a highly purified preparation of OCP in ice-cold acetone for 15 min as described in (Polívka et al. 2005). The precipitated protein was separated by centrifugation (8 min, 10,000 rpm). Since hECN is the only carotenoid in the OCP, the extracted pigment was used without further purification.

Absorption and fluorescence spectra

Measurement of absorption spectra

Absorption spectra were recorded using a Varian 2300 UV–Vis spectrophotometer. Prior to OCP spectra measurements, samples were either adapted to darkness for 20 min or—to induce the $OCP^o \rightarrow OCP^r$ phototransformation—illuminated for 10 min with intense, 1100 µmol photons m^{-2} s^{-1}, blue–green light (tungsten–halogen white light filtered through a 430–540 nm bandpass filter). The second derivative representation of the spectra includes a smoothing function. The experimental OCP^o spectrum was deconvoluted into two components using a custom-written Matlab script based on the Origin 6.1 deconvolution Program into Gaussians that employs a built-in function of minimizing the residual between the experimental data and the fitting function. For determination of the OCP^o and OCP^r amounts in the raw OCP^o spectrum the improved method of Polívka et al. (2013) was used. In contrast to the true OCP^o spectrum, the true absorption spectrum of the OCP^r is measurable (Wilson et al. 2008). This spectrum was modeled by the sum of the two Gaussians. The red end of the OCP spectrum has the region of OCP^r absorption only. Firstly, this long-wavelength region was modeled by the OCP^r and, after that, OCP^r was subtracted from the raw spectrum of OCP, obtaining the true OCP^o spectrum.

Determination of hECN extinction coefficient

The chromophore of OCP was released in acetone (see "Extraction of hECN" section), taken to dryness, and weighed quantitatively. To obtain all of the precipitated protein and pigment, the extraction procedure was repeated three times. The concentration of the precipitated protein in the sample was determined by the Lowry method. For comparative measurements of absorption and appropriate calculations, the molecular masses of hECN and OCP were taken as 582 and 34,600 Da, correspondingly (Wu and Krogmann 1997).

Measurement of fluorescence spectra

Fluorescence emission spectra were recorded with a Fluorolog-3 instrument (Horiba Jobin–Yvon). Samples were placed in a cuvette with 3-mm optical path; the measurements were carried out with excitation at 580 nm. The PBS fluorescence emission spectrum was deconvoluted into two components corresponding to the APC_{660} and APC_{680} pigment pools using a deconvolution program (see "Measurement of absorption spectra" section). Firstly, the spectrum APC_{660} was modeled by the two Gaussians and the spectrum of A680—by three Gaussians, correspondingly. For comparing the absorption and fluorescence spectra, their normalization, and calculation of the overlap integral, the nm scale was inverted to cm^{-1}.

Building of molecular models

The 3D attachments of OCP to the $(\alpha\beta)_2(PBL_{CM}\beta^{18})$ trimer of the PBS core and of OCP to the FRP were built using the Hex Protein Docking on-line service with standard settings (Ritchie et al. 2008). In the in silico modeling, proteins were considered as rigid bodies interacting through electrostatic and Van der Waals forces. The highest scored OCP–$(\alpha\beta)_2(PBL_{CM}\beta^{18})$ and OCP–FRP complex structures represented the most likely arrangement for these protein–protein assemblies. The GROMACS (Hess et al. 2013) software package was used to determine the area of the interaction interface by the SASA algorithm with a sample particle radius equal to 1.4 Å. The initial crystallographic

coordinates of OCP and FRP were obtained from Protein Data Bank (3MG1 for OCP^o from *Synechocystis*, 1.65 Å resolution) (Wilson et al. 2010) and 4JDX for FRP (2.3 Å resolution) from the same organism (Sutter et al. 2013). To achieve higher homological conformity in the docking procedure, because the crystal structure of APC trimers from *Synechocystis* is unknown, the coordinates for building the OCP–$(\alpha\beta)_2(PBL_{CM}\beta^{18})$ complex model were exploited with code 1M98 for OCP^o from *Arthrospira maxima* determined to 2.1 Å resolution (Kerfeld 2004) and code 1ALL for the APC from *A. platensis* (crystallographic resolution of 2.3 Å), a cyanobacterial species from the same genus *Arthrospira* (Brejc et al. 1995). Homology-based 3D molecular models of the PB polypeptide domain of L_{CM} including PB loop insertion and of ApcF (β^{18} polypeptide) were created using the MODELLER software (Baker et al. 2001). Coordinates of obtained earlier (Stadnichuk et al. 2013) 3D complex of OCP and homogeneous APC trimer were used as reference data to achieve smooth and careful geometry optimization of PBL_{CM} geometry with a standard automodel class for the whole structure model and loop-model class for a loop region (59–119 aa region). The phycobilin chromophore was placed in the corresponding apoprotein pocket that takes pyrrole ring A of phycobilin covalently bound to Cys198 to be turned through 180° to achieve chromophore position analogous to αAPC. The resulting computed chromophore coordinates were used to determine the distance between hECN in OCP and the nearest phycobilin pigment molecule belonged to PBL_{CM} and the vectors of transition dipole moments, correspondingly. All structural visualizations were performed using the PyMOL Molecular Graphics System (http://www.pymol.org).

MD simulations

MD simulations with the OCP–APC model was performed using the GROMACS software package and OPLS-AA (Jorgensen et al. 1996) force field with integration step of 1 fs and no constraints of hydrogen atoms. The initial coordinates were taken from PDB and the obtained docking model; electrostatic interactions were determined using a PME method with Fourier spacing 0.12 nm. Cutoffs of electrostatic and dispersion interactions were 1.25 nm; TIP4P model was exploited for water molecules. Models of cofactor molecules, hECN of OCP and phycocyanobilin of PBS, were also assembled from the atoms of standard for OPLS-AA types. For quantum chemical calculations, the FireFly software package (Granovsky 2014) based on source code of GAMESS US (Schmidt et al. 1993) was used. Molecular geometry optimization and subsequent calculation of molecular electrostatic potentials for pigment cofactors were carried out using the B3LYP5 functional in the 6 − 31 + G* basis set. For partial atomic charges of chromophore molecules, the quantum chemistry electrostatic potential was approximated by potential of point partial charges of atoms using the CHELPG method (Breneman and Wiberg 2004). Models of OCP, APC, and OCP–APC complex were dissolved in 27639, 71229, and 79298 water molecules in 9 × 9 × 11, 16 × 16 × 9, and 18 × 16 × 9 nm rectangular boxes, correspondingly. One hundred nanosecond MD simulations were performed for each system described above. All MD simulations were performed in periodic boundary conditions at 300 K and 1 Bar on the "Lomonosov" supercomputer of the Research Computing Center of Moscow State University.

Calculations of free energy by the MM-PBSA method

To estimate the free energy of the protein–protein structural interactions between OCP and APC in the obtained 3D model (Stadnichuk et al. 2013), the MM-PBSA method was used (Kollman et al. 2000). The total free energy of the OCP–APC complex formation, ΔG, was described as

$$\Delta G = G_{\mathrm{OCP-APC}} - G_{\mathrm{APC}} - G_{\mathrm{OCP}},$$

where $G_{\mathrm{OCP-APC}}$, G_{APC}, and G_{OCP} indicate full Gibbs free energy of the OCP–APC complex, APC, and OCP, correspondingly. Free energy of each protein system, G_{MOL}, was divided into several parts calculated separately:

$$G_{\mathrm{MOL}} = H_{\mathrm{MOL}} - S_{\mathrm{MOL}} + G_{\mathrm{SURF}} + E_{\mathrm{ION}} + E_{\mathrm{DEL}}.$$

Here, H_{MOL} is total macromolecule enthalpy, S_{MOL} is total macromolecule configurational entropy, G_{SURF} is free energy of the macromolecule–solute interface, E_{ION} is electrostatic energy of macromolecule ionization, and E_{DEL} is electrostatic energy of double electrical layer formation. The enthalpy, H_{MOL}, was estimated as total potential energy of the non-ionized macromolecule in vacuum from GROMACS simulations. Configurational entropy, S_{MOL}, was determined according to the normal modes frequencies spectra (Karplus and Kushick 1981). It appears to be small and was neglected, and as a consequence the change in internal macromolecular free energy was assumed to be equal to the protein enthalpy change. Solvation free energy, G_{SURF}, of each macromolecule was calculated semiempirically according to the SASA of a macromolecule from GROMACS simulations and normalized to the unit area free energies of dissolution of different chemical groups (Makhatadze and Privalov 1993). The ionization part of the macromolecular enthalpy, E_{ION}, and the energy of the double electrical layer formation, E_{DEL}, were calculated through the Poisson–Boltzmann equation solution using the APBS software with GROMACS geometry.

Transition dipole moments calculations

To calculate the S_1 and S_2 transition dipole moments and their unit vectors for hECN in OCP, the geometry of the chromophore molecule was optimized by density functional theory with the PBE functional and triple-zeta quality basis set 3z (PBE/3z) implemented in the "Priroda" program (Laikov 1997). The torsion angles between conjugated bonds of the polyene chain of hECN molecule from C7 to C33 carbon atoms were constrained to their experimental values from the Protein Data Bank according to 1M98 (3MG1) codes of OCP. The crystal structures of TRP290 (TRP288) and TYR203 (TYR201) residues of OCP hydrogen bonded to the carbonyl oxygen of hECN (Kerfeld 2004; Wilson et al. 2010) were also included in the computation. Their orientation with respect to the chromophore in the protein environment was also constrained. The electronic molecular states were calculated for the optimized geometry by the FireFly program (Granovsky) using the complete active space multiconfigurational self-consistent field method. The density matrix was averaged over the three lowest states, and the active space was 14 electrons on 12 orbitals (SA(3)-CASSCF(14,12)). Next, the energies were improved by second order extended multiconfigurational quasi-degenerate perturbation theory (XMCQDPT2) (Granovsky 2011). This method was chosen because the S_1 state of carotenoids can be formed after a double excitation and, therefore, cannot be calculated by TDDFT method, which includes only single excitation (Knecht et al. 2013). The $6-31+G^*$ basis set was used in these calculations. The transition dipole moment of the phycobilin S_1 state (PBL_{CM}) was verified under Förster theory using spectral data of fluorescence emission (Sinanoglou 1965) and the direction of the transition dipole moment was calculated following (Ren et al. 2013). For the mutual orientation of the hECN and the adjacent phycobilin chromophore of PBL_{CM} transition dipole moments the scaffold of hECN in OCP and of phycobilin in PBL_{CM} obtained in the 3D model of PBS and the OCP interaction was used.

Results

Free energy of OCP–APC complex formation from MD simulations

It is known that, for the majority of proteins, intermolecular contacts and packing in the crystal lattice are affected by the crystallization process. Besides, the rigid-body modeling of protein interactions using the Hex Protein Docking Server (Ritchie et al. 2008) or other docking software has thermodynamic restrictions. Therefore, before OCP–$(\alpha\beta)_2(PBL_{CM}\beta^{18})$ super-complex constructing it was necessary to verify the applicability of our previously developed model of the OCP–APC complex (Stadnichuk et al. 2013) to the OCP-dependent NPQ process by all-atom MD simulations and subsequent thermodynamic analysis. We have used a 3D structure of the OCP orange form, as in (Stadnichuk et al. 2013; Zhang et al. 2014) because the red form of OCP is not yet crystallized and its spatial structure is not revealed. Nevertheless, we propose that OCP^r structure is quite similar to the structure of OCP^o (Zhang et al. 2014).

Table 1 demonstrates the results of the free energy calculations performed for the OCP–APC complex. The MM-PBSA approach allows separate calculation of changes in protein enthalpy (which is predominantly equal to protein free-energy change), the free energy of protein–water interaction that is a simple free energy of water-exposed protein surface, and polarization energy. The data, in all three cases, indicate the very large absolute values of enthalpy, surface, and polarization energies determined for individual OCP, APC, and the formed OCP–APC complex (Table 1). The large energy values are predicted by the large total volume and large surface area of both protein macromolecules and the formed OCP–APC system. At the same time, relative deviations of the resulting numerical values are very small, indicating high stability of the molecular models in MD simulations. As a result of water displacement from the protein surface, total free energy of protein complexation appears to be positive and equal to $\sim$470 kJ/mol. In a good agreement with this result, the GROMACS enthalpy of OCP–APC complex formation is negative and equal to about –400 kJ/mol, indicating complementarity of two molecular surfaces forming the contact area. The contribution of protein molecule ionization and solvent polarization to the free energy of complex formation is about one order of magnitude less and also negative (–60 kJ/mol). Thus, the summed negative contributions to total free energy of OCP–APC complex formation is found to be almost equal to the positive energy loss related to the corresponding decrease in the water–protein interface in the OCP–APC complex (Table 1). That is why the resulting free energy of OCP–APC complex formation is smaller than its own deviation. Twelve water molecules were revealed in the hECN–APC interface during MD simulations procedure that is two molecules more than located in the vicinity of hECN in 1M98 crystal structure of the OCP. They form two clusters of 8 and 4 H_2O molecules: (1) between the hECN and aminoacid residues of APC and (2) between the hECN and R155–E244 salt bridge of the OCP, correspondingly. Three of them are located in positions similar to the water molecules #411, 452 and 628 of 1M98. Two water molecules form hydrogen bonds with the R155 residue and two another water molecules form a hydrogen bonds with E244 residue. The rest five H_2O

Table 1 Free energy (kJ/mol) of OCP, APC, and OCP–APC complex formation from MM-PBSA calculations

	OCP	APC	OCP-APC	Difference
H_{MOL}	−25,800 ± 10	−80,300 ± 10	−106,500 ± 10	−400 ± 70
G_{SURF}	−8870 ± 10	−21,530 ± 10	−29,930 ± 10	470 ± 70
$E_{ION} + E_{DEL}$	2020 ± 20	5840 ± 30	7800 ± 40	−60 ± 50
G_{MOL}	−32,650 ± 30	−95 990 ± 50	−128,630 ± 60	10 ± 70

G_{MOL} total free energy, H_{MOL} the GROMACS enthalpy, G_{SURF} the surface free energy of the systems, $E_{ION} + E_{DEL}$ the polarization energy

molecules are hydrogen bonded to water molecules enumerated above. The salt bridge between R155 and E244 was flexible but was preserved during all the time of MD simulations procedure. In common, the composition of water molecules surrounding hECN chromophore inside the OCP central cavity did not undergo any crucial changes in APC–OCP complex comparing with the crystal structure of OCP (1M98). Compared to the estimated OCP and APC total free energies, the calculated very small value of complexation free energy would appear to indicate very loose association between the OCP and $(\alpha\beta)_3$ of APC. Thus, it appears that chemical forces that lead to assembly do not induce the formation of very strong intermolecular interactions. Loose association between the two protein components corresponds well to reversibility of the OCP-mediated NPQ in cyanobacteria that excludes unnecessary stable complex formation. On the other hand, in our model the forced by absence of X-ray data replacement of OCP^r to OCP^o and of PBL_{CM} to αAPC could easily change through some corresponding conformational rearrangements the sign and the absolute value of the determined free energy. In this sense, the obtained small module value of complexation free energy is of much greater importance than the inaccuracy of its exact calculated value (Table 1). This result suggests that there could be a weak interaction between the OCP^o and PBS that was not previously detected. Taking into account a very small absolute value of the free energy obtained in calculations, the corresponding binding constant should be in the range of 10^2–10^3. This value is too small to detect it for macromolecules like OCP and the more so the PBS. The known detectable binding constant values for proteins with molecular masses of hundreds kDa are known to dispose in the range of 10^5–10^6, which requires a binding free energy in the range of 30–40 kJ/mole. Such a value is quite possible for the OCP^o/PBS complex according to the MD simulations and MM-PBSA free energy calculation (10 ± 70 kJ/mole); consequently, the real value has to be closer to zero or even more positive than our calculated value. Finally, it was concluded that MD simulations are not at variance with the thermodynamic possibility of the in silico OCP and PBS super-complex formation using the crystal structures of the corresponding proteins.

Molecular model of OCP–PBS interaction

Constructing of a 3D model where OCP and PBS stick together owing to the PBL_{CM} domain is necessary to derive any conclusions about the molecular mechanism of OCP-induced fluorescence quenching. Due to the bulky PBS superstructure, it was not clear a priori where and how the OCP could attach to the PBS core, and there were many constraints to be taken into account including the shape of both OCP and PBS. Nevertheless, the lateral surface of the APC cylinders, in contrast to the butt of the central channel, is not occupied by linker polypeptides, $L_{7.8}$ (Adir 2005; Watanabe and Ikeuchi 2013), and, therefore, could easily be accessed by other proteins. Our realized previously docking of the OCP to the homogenous APC trimer (Stadnichuk et al. 2013) accompanied by subsequent MD simulations and thermodynamic analysis (see "Free energy of OCP–APC complex formation from MD simulations" section) provided a strong possibility of OCP attachment at the site that includes both the α- and β-subunits of APC. The resulting 3D model of the OCP–APC complex where the central cavity of OCP molecule and the characteristic tip from the outer side of APC trimer tightly conform to each other (Fig. 1a and Stadnichuk et al. 2013) was assumed as the reference structure for the modeling of OCP interaction with the PBL_{CM} domain which is an organic part of $(\alpha\beta)_2(PBL_{CM}\beta^{18})$ trimer within the bottom APC cylinders of the PBS core.

Because there are no crystallographic data for the PBL_{CM} domain and for β^{18}APC as well as for the whole $(\alpha\beta)_2(PBL_{CM}\beta^{18})$ trimer, we utilized the possibility of their computer modeling. The amino acid sequences show that the β^{18} polypeptide is highly homologous to the APC β-subunit while the primary structure of the PBL_{CM} domain is similar to that of αAPC (Adir 2005; Watanabe and Ikeuchi 2013). The 3D structure of the β^{18} polypeptide built in this work through homology modeling using MODELLER software (Baker et al. 2001) was found to be highly similar to the crystal structure of the APC β-subunit (Fig. 1b). Analogously, a homology-based 3D model of the chromophorylated PB domain of L_{CM} (Stadnichuk et al. 2013; McGregor et al. 2008; Gao et al. 2012) created through homology modeling with the use of α-subunit of APC as a

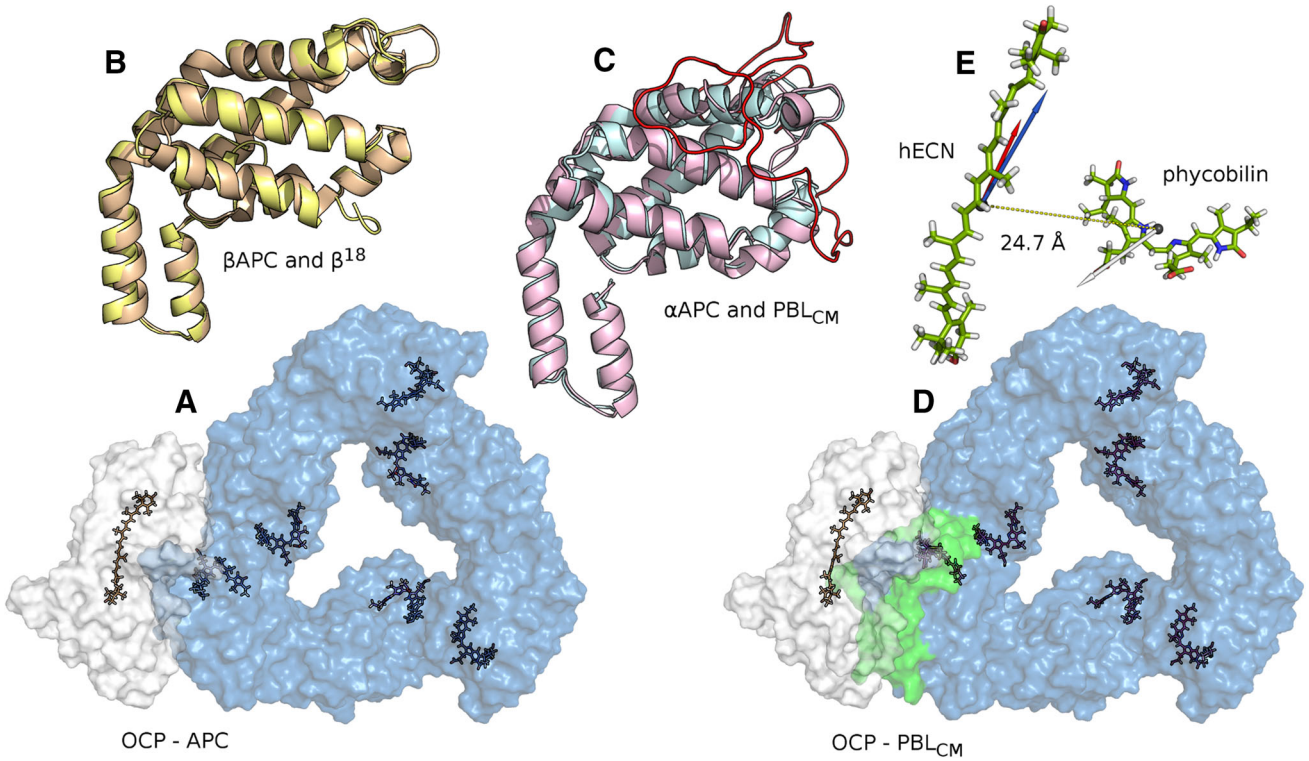

Fig. 1 A proposed model for the OCP–PBS interaction. **a** Possible docking of the monomeric form of OCP (*white*) to the APC trimer (*blue*); here and in Fig. 1D hECN and phycobilin chromophores are shown as *black sticks*. The figure is reproduced from (Stadnichuk et al. 2013). **b** A homology-based similarity model of the β^{18} polypeptide (*yellow*) and βAPC (*orange*). **c** A homology-based stereo model demonstrating high structural similarity between the PB domain of L_{CM} (*pink*) including the folded PB loop (*red*) and αAPC (*blue*); the phycobilin chromophore here and in Fig. 1b is extracted for clarity. **d** The model of OCP attachment to the $(\alpha\beta)_2(PBL_{CM}\beta^{18})$-trimer of the PBS core; the region of the folded PB loop is designated by *green* and *semi-transparent green*. (E) The hECN and the nearby phycobilin of PBL_{CM} in their protein binding pockets enlarged and extracted from Fig. 1**d**. The determined center-to-center of masses distance is indicated. Vectors of the transition dipole moments are designated by *arrows*. The $S_0 \leftrightarrow S_1$ (*red arrow*) and $S_0 \leftrightarrow S_2$ (*blue arrow*) transition dipole moments of hECN are calculated to be ~20° apart; the scalar scale of the arrows is not maintained

reference structure demonstrated its conformation to be similar to that of αAPC (Fig. 1c). After all, one of the β–polypeptides was virtually extracted from the ring structure of the APC trimer disk (presented in Fig. 1a) and substituted by the built homologous 3D model of β^{18} using the MODELLER software. Analogously to β^{18}, using the same software, the extracted αAPC in constructed model was substituted by PBL_{CM}. As an intermediary energy converter to PBL_{CM} from the bulk APC, the β^{18} in the trimer model is the nearest neighbor of PBL_{CM} with closest apposition of their chromophores. (Adir 2005; Watanabe and Ikeuchi 2013). In contrast to high similarity of the β^{18} and βAPC subunits, PBL_{CM} differs from αAPC in a significant detail. The PB domain is contained in the *N*-terminal part of the ~900 aa. L_{CM} protein (residues 1–240) (Capuano et al. 1991) and has an approximately 60-residue insertion called the PB loop, which is of presently unknown function. The deletion of the PB loop does not influence the PBS assemblage, the attachment of PBS to the thylakoid membrane, and energy transfer from PBS to chlorophyll (Ajlani and Vernotte 1998). Also, it does not attribute to auto-chromophorylation of L_{CM} (Gao et al. 2012). So, we proposed that the function of the PB loop could be as a participation in OCP attachment. Also a good argument in favor of this assumption is the location of PB loop exactly in the region of the tip that possibly interacts with the OCP. The realized folding of the PB loop in the frame of the modeling procedure strengthened this assumption (Fig. 1d). The central cavity region in the interface of the *N*- and *C*-terminal domains of the OCP contains plenty of water molecules (Wilson et al. 2008; Rakhimberdieva et al. 2010). The PB loop adjoins OCP, supplants the water inside the OCP cavity, and therefore enlarges the calculated total contact area with OCP from 2600 $Å^2$ in the constructed OCP–APC complex (Fig. 1a) to 3900 $Å^2$, in the OCP–$(\alpha\beta)_2(PBL_{CM}\beta^{18})$ complex (Fig. 1d), correspondingly. The highly conserved Cys84 residue, which is a covalent attachment point for the phycobilin cofactors in APC and all other phycobiliproteins, is absent in PBL_{CM} and is replaced with serine residue. Phycobilin molecule is bind to the alternative cysteine residue (Cys190

or Cys198 in *Synechocystis* and *Arthrospira*, correspondingly), which is located on the opposite side of the chromophore-binding pocket (Fig. 1d and McGregor et al. 2008; Gao et al. 2012). Because of the PB loop folding and the presence of surrounding polar amino acids the phycobilin molecule in the PB domain is pulled closer to the outside surface of the protein, bringing it nearer to the hECN chromophore of the OCP. The closest distance between the two pigment cofactors was determined to be ~14 Å, with distance between the centers of mass equal to 24.7 Å (Fig. 1e).

Molecular model of OCP–FRP interaction

The main geometric feature of OCP is the presence of two structural domains, the all α-helical *N*-terminal domain and the α/β-composed *C*-terminal domain, and a large surface cavity located in between them and leading to the carotenoid-binding cleft (Fig. 2a and Kerfeld 2004; Wilson et al. 2010). The obtained 3D models of the complex formed by OCP with the $(\alpha\beta)_2(PBL_{CM}\beta^{18})$-trimer (Fig. 1D) and/or $(\alpha\beta)_3$-trimer of APC (Fig. 1a and Stadnichuk et al. 2013) revealed the decisive importance of the central cavity of the OCP in the OCP–PBS interaction. Remarkably, the cavity surface faces ideally toward a very characteristic tip jutting from the lateral bulge of both varieties of PBS core-trimers. Their resulting 3D design verified the role of the intra-domain cavity of the OCP in another known interaction of OCP with the FRP during restoration of normal antenna capacity of the PBS (Boulay et al. 2010).

In contrast to OCP and APC containing both α- and β-polypeptide fragments, the small FRP consists only of α-helices and short disordered loops that connect α-helices and form an extended helical stalk and a compact head domain (Sutter et al. 2013). In the resulting 3D crystal structure the FRP was found in dimeric and tetrameric states. Efforts to generate the tetramer in solution by varying pH and salt concentration were not successful; the dimer form (Fig. 2) is predominant, and the larger form might be a dimer of dimers (Sutter et al. 2013). Therefore, following (Sutter et al. 2013), we have proposed that the four-helix bundle corresponding to a tetramer and observed in the crystal structure of FRP is a side effect of the concomitant crystallization procedures, and performed docking of full-length FRP monomer and FRP dimer with the OCP molecule. As in the case of OCP–PBS complex construction, we used the orange form of OCP instead of OCP^r since the OCP red form structure is presently unknown. We propose that the structures of OCP^r and OCP^o are quite similar for our purposes (Zhang et al. 2014). The most convincing solution based on score and surface complementarity places the FRP monomer binding site at the same central surface cavity of the OCP monomer as the $(\alpha\beta)_2(PBL_{CM}\beta^{18})$-trimer does (Figs. 1d and 2). The total area of protein–protein interaction interface between the monomeric forms of OCP and FRP was about 2550 $Å^2$, which makes it equal with the interface of possible OCP and APC trimer interaction. The striking feature of this model is the complete similarity of the interaction interface of OCP and the ~100 kDa APC trimer with the interface of OCP and the FRP (only 13 kDa). In this interaction, the head domain of the FRP molecule plays the role of APC tip. Tested by co-immunoprecipitation, the interaction between the *C*- and *N*-terminal domains of the OCP with FRP had shown that only the *C*-terminal domain coprecipitates with the FRP (Kirilovsky and Kerfeld 2013). This result correlates with our model (Fig. 2) where the *C*-domain of the OCP interacts both with head and stalk domains of the FRP, while the *N*-terminal domain is in contact only with a some small part of its head domain. We then expanded the docking refinement to the FRP dimer and found an interface as well. The solution resulting from docking of OCP with the FRP dimer demonstrated a lower surface-binding

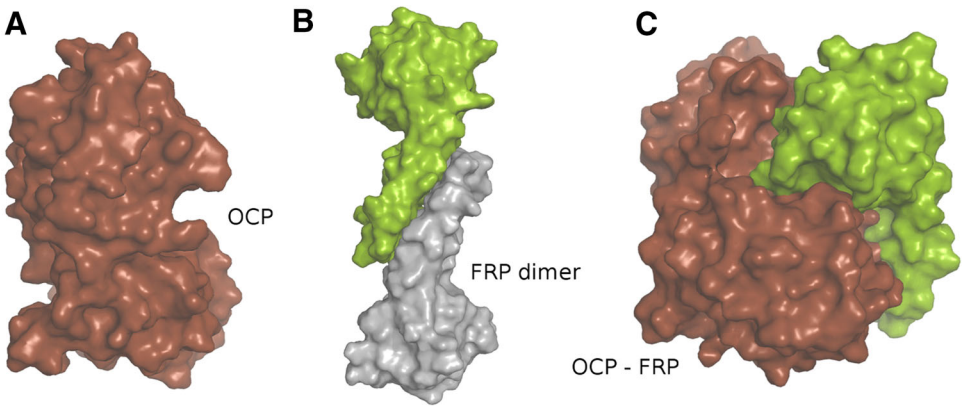

Fig. 2 Proposed 3D model for the interaction of OCP and FRP demonstrating the role of the central cavity of OCP as the attachment site for an FRP molecule. **a** 3D structure of OCP according to 3MG1 code of PDB. **b** 3D structure of FRP dimer according to 4JDX code of PDB; two identical monomers of the dimer are shown in *green* and *gray* for clarity. **c** Proposed 3D model of OCP and FRP monomer binding

region and therefore was admitted less well (data not shown).

Properties of absorption spectra of OCP

The obtained 3D attachment model reveals a sufficiently low separation distance between the carotenoid chromophore of OCP and the phycobilin chromophore of the PBL_{CM} domain (Fig. 1d and e). Therefore, we proposed that hECN of the OCP could directly interact with the neighboring phycobilin chromophore(s) of the PBS and dissipate the absorbed energy. To test this assumption, the spectral properties of the OCP and molar extinction coefficient of hECN need to be defined more properly. For quantitative determination of hECN, the standard carotenoid extraction in acetone from photosynthetic tissues was used. The absorption spectrum of OCP^o with main peak at 496 nm (Fig. 3a) has been repeatedly described in the literature (Polívka et al. 2013 and references therein). After extraction, the height of the peak of hECN was invariable although blue-shifted to 460 nm (Fig. 3a). This means that, in OCP, noncovalently bound hECN does not change its extinction (measured at peak position, not integrating over the entire wavelength range). Taking into account the only carotenoid chromophore present in OCP, we evaluated its extinction coefficient to be 110 mM^{-1} - cm^{-1}. Various carotenoids do not differ appreciably in their absorption properties. To estimate the concentration of free carotenoids in the eluent or the stoichiometry of carotenoid to protein, an average extinction coefficient of $\geq 10^2$ mM^{-1} cm^{-1} is usually applied (Gall et al. 2005). Particularly, for hECN in the OCP the coefficient of $2500^{1\ \%}$ cm^{-1} (Holt and Krogmann 1981) or 132 mM^{-1} cm^{-1} (Stadnichuk et al. 2013) was used. Our specific estimation fully corresponds to these values.

A characteristic three-peak band shape caused by the vibrational structure of the strongly allowed $S_0 \rightarrow S_2$ transition is the dominant feature of carotenoid absorption spectra. These peaks are attributed to the 0–0, 0–1, and 0–2 vibrational transitions based on the assignment of a single dominant C=C stretching mode (Polívka et al. 2005). Besides the 0–0 vibrational peak located at 496 nm, OCP^o has a second peak at 467 nm with a shoulder at about 440 nm (Fig. 3a). The experimental absorption spectrum of hECN in OCP^o does not resemble a typical carotenoid absorption spectrum (Polívka et al. 2013) because hECN in OCP^o has its absorption maximum at the 0–0 band. In contrast, essentially all absorption spectra of carotenoids in solution reported to date, including the hECN spectrum, have absorption maximum at the 0–1 vibrational band (Polívka et al. 2013). Under ambient light an equilibrium is established between OCP^o and OCP^r in vivo (Ren et al. 2013) and in vitro (Polívka et al. 2013). The red-shifted spectrum

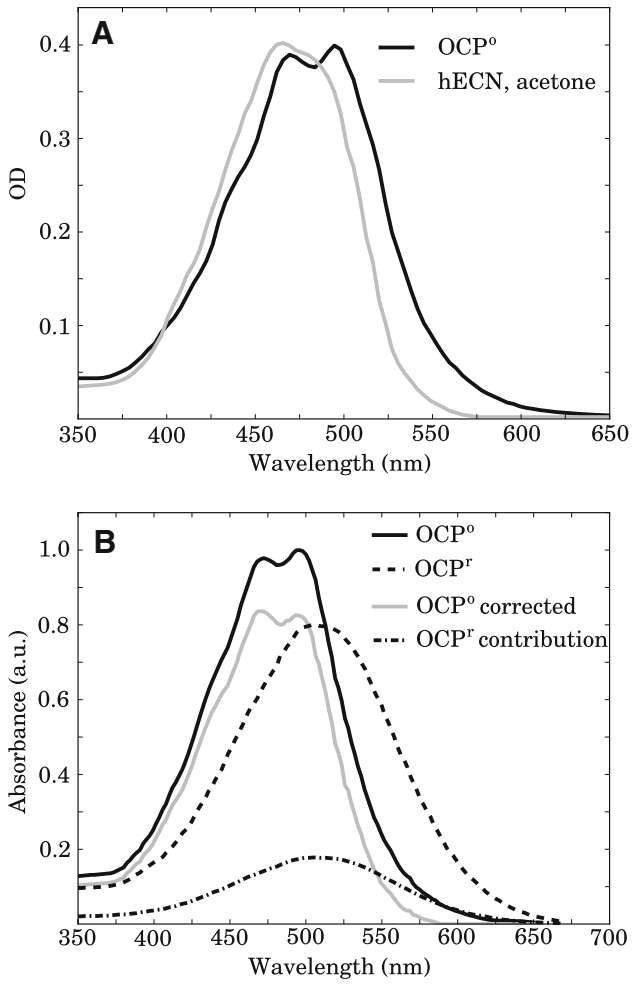

Fig. 3 **a** Absorption spectrum of OCP^o (*black*) compared with the absorption spectrum of hECN in acetone quantitatively extracted from the same OCP sample (*gray*). The approximate absorbance of both samples was 0.8 OD in a 1 cm path. **b** Absorption spectra of OCP^o (*solid*, *black*), OCP^r (*dotted*, *black*), subtracted part of OCP^r from the experimental spectrum of OCP^o (*dashed*, *black*) and estimated spectrum of OCP^o, obtained by subtraction of the OCP^r band from the experimental spectrum of OCP^o (*solid*, *gray*)

of the OCP^r form loses the resolution of the vibrational bands and presents only one flattened peak at 509 nm (Fig. 3b and Wilson et al. 2008). We obtained the true absorption spectrum of the photoinactive dark OCP^o form after its deconvolution into two parts and subtraction of the long-wavelength broader band due to the OCP^r spectrum. This procedure demonstrated that the 0–1 vibrational band dominates the absorption spectrum of OCP^o as well (Fig. 3b). Earlier an analogous procedure was used after deconvolution of the absorption spectrum of OCP^o into a sum of Gaussian bands and subtraction of the reddest band presumably due to OCP^r (Polívka et al. 2013). To define more exactly the resolution of the three vibrational bands, the second derivative absorption spectrum of OCP^o was

obtained (Fig. 4a). All three peaks were well resolved, and an additional small peak at 406 nm to the blue of the 0–2 vibronic band was revealed. The use of derivative spectroscopy was most useful in the case of OCP^r. The flattened absorption maximum in the initial absorption spectrum was resolved into 0–0 and 0–1 peaks of 526 and 496 nm, correspondingly, and the third one, the 0–2 vibrational band at 470 nm, was clearly seen too (Fig. 4b). Therefore, the energy shift between the 0–0 vibrational peaks of OCP^o at 496 nm (20,160 cm^{-1}) and OCP^r at 526 nm (19,010 cm^{-1}) turned out to be bigger than proposed earlier comparing the initial absorption spectra of the photoactive and photoinactive OCP forms.

Fluorescence emission spectrum of PBL_{CM}

The objective of this section is to characterize the acceptable fluorescence emission spectrum of L_{CM} within the intact PBS. The L_{CM} can be isolated, but, like other free PBS linkers, it is nearly insoluble in most buffers and is kept in solution in the presence of urea or dilute acids (Zhao et al. 2005 and references therein). The dissoluble L_{CM} is already partly denatured, based on the lowered absorption ratio of the visible and the near-UV band and blue-shifted peak positions of its visible absorption and fluorescence emission spectra (Zhao et al. 2005). In native PBS, L_{CM} and ApcD appear to have very similar fluorescence emission spectra, with room temperature maximum emission at 680 nm (Gindt et al. 1994). It is generally accepted that the fluorescence emission spectrum of the PBS core can be ascribed to the two main pigment pools (Tian et al. 2012). One of them denoted as APC_{660} corresponds to bulk APC trimers, and the other one denoted as APC_{680} is stipulated by the long-wavelength PBS terminal emitters with the main contribution to L_{CM}. To simplify the problem, the APC_{660}- and APC_{680}-parts of the PBS fluorescence spectrum could be modeled by Gaussian components (Kuzminov et al. 2012). We registered the fluorescence emission spectrum of the PBS from the *Synechocystis* CK mutant devoid of C-phycocyanin and therefore fully ascribed only by APC_{660} and APC_{680} spectral components (Fig. 5). In our two-component-deconvolution procedure, the experimental spectrum of isolated APC was used as the starting value for the APC_{660} short-wavelength component instead of a Gaussian band. The second, long-wavelength component after fitting has peak position at ~680 nm and was used as the fluorescence emission spectrum of PBL_{CM} in subsequent calculations of energy migration. The fitting procedure demonstrates that the APC_{660}- and APC_{680}-components are strongly overlapping in all the spectral region of

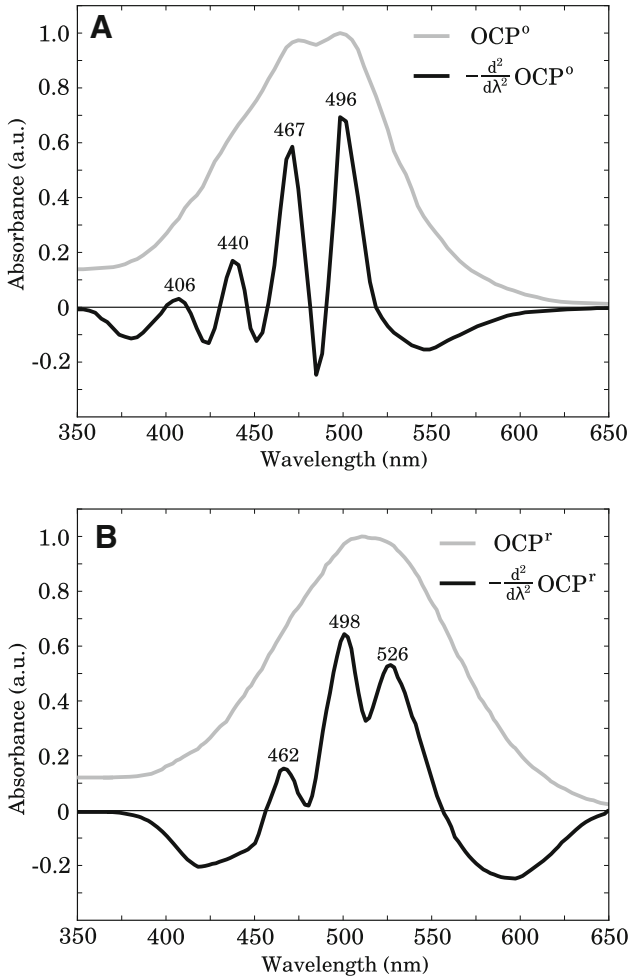

Fig. 4 Absorption spectra (*gray*) of OCP^o (**a**) and OCP^r (**b**) and their second derivatives (*black*)

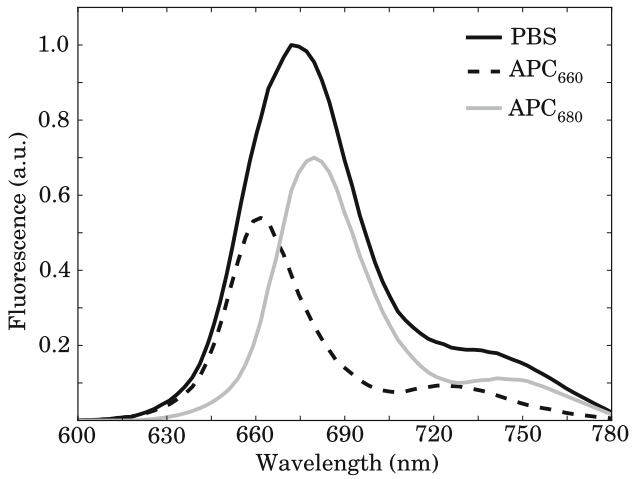

Fig. 5 Fluorescence emission spectrum of PBS from the CK mutant of *Synechocystis* devoid of lateral C-phycocyanin cylinders; excitation of the sample at 580 nm. The spectrum is deconvolved into two components that correspond to the bulk APC (APC_{660} pool) and PBL_{CM} (APC_{680} pool)

fluorescence emission, and relatively less fluorescence originates from higher energy chromophores than from 680 nm emitters (Fig. 5).

Energetic coupling between hECN of OCP and the phycobilin chromophore of PBL_{CM}

Carotenoids play a crucial role in the energy dissipation processes in photosynthetic antennas. The electronic coupling between S_1 and/or S_2 energy states of various carotenoids and chlorophyll or bacteriochlorophyll molecules in light-harvesting complexes is well documented (for references see, e.g., Holleboom and Walla 2014). The evidence exists for both energy and electron transfer quenching in NPQ processes in higher plants and diatomic algae but, generally, there is no single mechanism of NPQ for natural photosynthetic systems (Kloz et al. 2011; Holleboom and Walla 2014; Ruban et al. 2014). Three mechanisms of tetrapyrrole singlet excited-state quenching were identified in artificial dyad systems: (i) tetrapyrrole–carotenoid electron transfer and recombination; (ii) tetrapyrrole to carotenoid S_1 energy transfer and fast internal conversion to the carotenoid ground state; (iii) excitonic coupling between tetrapyrrole and carotenoid S_1 states and ensuring internal conversion to the ground state of carotenoid (Kloz et al. 2011; Liao et al. 2011). The water-soluble OCP is recognized to be an ideal minimal system to study the interaction between a single carotenoid in its protein environment and quenched chromophore molecule(s) revealing the entire photophysical quenching process (Kirilovsky and Kerfeld 2013). The availability of the geometrical model of OCP and PBL_{CM} cooperation (Fig. 1d) allows study of the OCP-dependent NPQ on the basis of the exact mutual arrangement of the interacting chromophores. We do not examine the mechanism of electron transfer because the estimated inter-chromophore distance of 24.7 Å (Fig. 1e) makes this chance very improbable. To complete the patterns of possible energy heat dissipation, the subject of this section is the partition of the energy flow from PBL_{CM} to the S_1 and S_2 energy states of hECN in OCP and the role of both states in NPQ feasibility.

Possible role of S_2 energy state of hECN in energy quenching

Based on well-known Förster theory, electronic excitation transfer (EET) efficiency determines the extent of donor quenching due to the acceptor. Ideally, the theory is applicable to a donor–acceptor dyad separated by a fixed distance (Lakowicz 2006) and the case of OCP-induced quenching fits this situation best. The greater the overlap of the emission spectrum of the donor with the absorption spectrum of the acceptor, the higher is the rate of energy transfer. The experimental spectral data provide direct observation of the $S_0 \rightarrow S_2$ OCP absorption (acceptor) and PBL_{CM} emission (donor) from which the spectral overlap integral between the hECN in OCP and phycobilin in PBL_{CM} can be examined. The S_1 energy level of the PBL_{CM} chromophore lies below the high-lying S_2 energy level of hECN of OCP, but the $S_0 \rightarrow S_2$ absorption spectra of both OCP^o and OCP^r are very extended to the red. Comparison of fluorescence emission and absorption spectra of these pigments on the energy scale (Fig. 6) indicates that the spectrum of PBL_{CM} is really separated from the absorption spectrum of OCP^o but overlaps with the low-energy falling edge of the spectrum of OCP^r. The overlap is small, but the determined high extinction coefficient of hECN in the blue–green spectral region ($110\ mM^{-1}\ cm^{-1}$) requires taking it into consideration when we should also consider thermal fluctuations in the relative state energies for the process of reverse energy transfer.

Förster theory (Sinanoglou 1965; Lakowicz 2006) determines the effectiveness of energy transfer under the assumption that the relevant interaction between donor and acceptor can be approximated by the leading dipole–dipole term (inductive-resonant mechanism). Following Förster, the rate constant k_m of electronic energy transfer between donor (D = phycobilin chromophore of PBL_{CM}) and acceptor (A = hECN of OCP) is given by the equation

$$k_m = \frac{\pi\chi^2}{R^6} \int \frac{p_D^2 p_A^2}{\hbar^2} G_D(\tilde{\nu}) G_A(\tilde{\nu})\, d\tilde{\nu} \qquad (1)$$

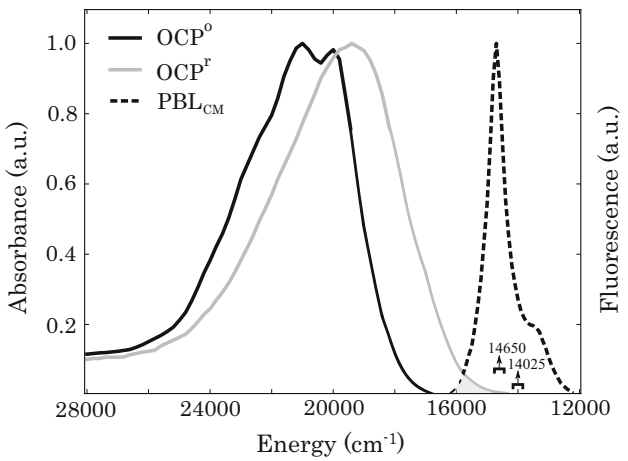

Fig. 6 Absorption spectra of corrected OCP^o (*black*) and OCP^r (*gray*) in the $S_0 \rightarrow S_2$ absorption region and fluorescence emission spectrum of PBL_{CM} (*black*, *dotted*). The spectral overlap integral area is shaded in gray. Spectra are compared on the energy scale (cm^{-1}) and normalized at their peak positions. The S_1 energy values of hECN in OCP^o and OCP^r (according to Polívka et al. 2013) are designated by *vertical arrows* with error bars depicted by rectangle brackets

Here, R is the distance between centers of mass of donor and acceptor, p_D and p_A are the magnitudes of the transition dipole moments, correspondingly, $\tilde{\nu}$ is a wavenumber, and χ is the transition dipole–dipole orientation factor (so-called form-factor) which is given by

$$\chi = 3\cos\theta_A \cos\theta_D - \cos\varphi_{AD}, \tag{2}$$

where φ_{AD} is the angle between the emission transition dipole moment of the donor and the absorption transition dipole moment of the acceptor, and θ_A and θ_D are the angles between these dipoles and the vector joining them. $\int$ is the overlap integral (the spectra overlap part) between the donor fluorescence $G_D(\tilde{\nu})$ and the acceptor extinction $G_A(\tilde{\nu})$. The functions $G_D(\tilde{\nu})$ and $G_A(\tilde{\nu})$ represent the spectral area-normalized fluorescence and absorption line shapes (the line shape functions, each normalized to unit area on a wavenumber scale):

$$\int G_D(\tilde{\nu})\, d\tilde{\nu} = \int G_A(\tilde{\nu})\, d\tilde{\nu} = 1. \tag{3}$$

The function $G_D(\tilde{\nu})$ is associated with an experimental function $F_D(\tilde{\nu})$ which is the normalized spectrum of the donor fluorescence emission as following:

$$G_D(\tilde{\nu}) = B_D \frac{1}{p_D^2} \frac{F_D(\tilde{\nu})}{\tilde{\nu}^3}, \tag{4}$$

where $B_D = \frac{3\hbar}{32\pi^3 n^3 \tau_D}$, n is the refractive index of the surrounding medium, and τ_D is the excited-state lifetime of the donor molecules in the absence of the acceptor. Similarly, the function $G_A(\tilde{\nu})$ is associated with a molar extinction coefficient $\varepsilon_A(\tilde{\nu})$:

$$G_A(\tilde{\nu}) = B_A \frac{1}{p_A^2} \frac{\varepsilon(\tilde{\nu})}{\tilde{\nu}}, \tag{5}$$

where $B_A = \frac{3000\ \ln 10\ \hbar\, c}{4\pi^2 N_A n}$, and N_A is Avogadro number. Using the quantum yield of the donor fluorescence emission in the absence of the acceptor, Φ_D, we substitute Eqs. 4 and 5 into Eq. 1. As a result the transfer rate constant, k_m, can be presented in standard form:

$$k_m = \frac{9000 \ln(10) \chi^2 \Phi_D}{128\pi^5 N_A \tau_D R^6 n^4} \int F_D(\tilde{\nu}) \varepsilon_A(\tilde{\nu}) \tilde{\nu}^{-4} d\tilde{\nu}. \tag{6}$$

The Förster radius is the distance between the donor and acceptor where electron transfer is 50 % efficient, i.e., $k_m \tau_D = 1$. From Eq. 6 for the Förster radius, R_0, one can obtain:

$$R_0^6 = \frac{9000 \ln(10) \chi^2 \Phi_D}{128\pi^5 N_A n^4} \int F_D(\tilde{\nu}) \varepsilon_A(\tilde{\nu}) \tilde{\nu}^{-4} d\tilde{\nu}. \tag{7}$$

Since the characteristic migration time is determined as $\tau_m = k_m^{-1}$, combining Eqs. 6 and 7 we obtain Eq. 8 convenient for determination of the time of energy migration from the donor to acceptor, τ_m:

$$\tau_m = \tau_D \left(\frac{R}{R_0}\right)^6, \tag{8}$$

where $\tau_m = k_m^{-1}$ is the characteristic time of energy migration. Therefore, the radius R_0 and the time τ_m can be calculated from the known normalized experimental functions $F_D(\tilde{\nu})$ and $\varepsilon_A(\tilde{\nu})$. The useful application of the Förster theory is determination of the transition dipole moment magnitude of the donor molecule, p_D, from the normalized experimental fluorescence emission spectrum. It can be calculated on the basis of Eqs. 4 and 3 as:

$$p_D = \sqrt{B_D \int F_D(\tilde{\nu}) \tilde{\nu}^{-3}\, d\tilde{\nu}}. \tag{9}$$

The quantum yield of fluorescence for PBS and APC is known to be 0.5–0.68 (Holzwarth 1992 and references therein); for our calculations, an average value of $\Phi_D = 0.60$ was used. The refractive index of the surrounding medium, n, was set to 1.6 on the basis of known experimental results (Matamala et al. 2007); the intrinsic time of donor (PBS) emission is known to be $\sim$1800 ps (Holzwarth et al. 1990). The dipole–dipole orientation coefficient (a factor χ of relative orientation of donor and acceptor dipole transition moments) calculation needs the determination of the direction of the dipole moment of the chromophores (the angles in Eq. 2). According to our quantum chemical calculations, the $S_0 \leftrightarrow S_1$ and $S_0 \leftrightarrow S_2$ hECN transition dipole moments were found to point along the conjugated portion of the carotenoid molecule from the crystal structure (Fig. 1e). As for the PBL_{CM} donor, the vector of phycobilin dipole transition moment forms the non-perpendicular angles with the directions of $S_0 \leftrightarrow S_1$ and $S_0 \leftrightarrow S_2$ hECN transition dipole moments (Fig. 1e). This suggests orientation factors value of $|\chi| \approx 0.24$. The calculated overlap integral, using the normalized spectral distribution of a donor emission and the spectral distribution of an acceptor molar extinction coefficient in the range of spectral overlap (Fig. 6) exhibits a value of $\int = 1.17 \times 10^{-14}$ cm^3 M^{-1} (see Eq. 1). The calculation of Förster radius (see Eq. 7) resulted in $R_0 = 25.2$ Å. Therefore, according to Eq. 8, τ_m was determined as $\sim$1450 ps. This is less than the intrinsic lifetime of the donor (1800 ps), but in a cyanobacterial cell the OCP-induced quenching has to compete with the time of energy migration from the PBS to the reaction centers of $\sim$200 ps (Sharkov et al. 1994). As this is not likely, this value demonstrates that we have obtained evidence for the non-participation of the S_2 state of hECN in OCP in the process of PBS quenching.

In the literature, exists the alternative hypothesis that the bulk APC (APC_{660}) is being quenched (see, e.g., Tian et al. 2011; 2012). Whereas this supposition contradicts to the

absence of OCP and APC_{660} interaction in vitro (Stadnichuk et al. 2012), the spectral overlap of the APC660 emission with the OCP^r absorption in the region of $S_0 \rightarrow S_2$ transition is larger. Therefore, it was interesting to calculate the time of possible energy migration in this case too. Analogous calculations for APC_{660} pigment pool exhibit the overlap integral value of $\int = 4.01 \times 10^{-14}$ cm^3 M^{-1}, the Förster radius of $R_0 = 29.5$ Å, and the time of migration τ_m equal to 610 ps. Although this time is less than in the first case it is too large to induce the quenching and makes this theoretically possible assumption not likely.

Role of S_1 energy state of hECN in energy dissipation

Carotenoids, along with polyenes, have an unusual structure of electronic excitations, a high-lying, absorbing state S_2, and a low-lying having the same symmetry as the ground state S_1 state. The S_1 state is dipole-forbidden via one-photon transitions and therefore is absent from linear absorption measurements. According to traditional Förster theory, energy transfer rates that involve the carotenoid S_1 state should be rigorously zero because of the zero transition dipole moment of the latter. Transfer from the optically forbidden S_1 state cannot occur via the Förster mechanism which requires the participating states to be allowed (Ritz et al. 2000). Nevertheless, it has been demonstrated experimentally many times that in natural and artificial light-harvesting systems carotenoids S_1 to chlorophyll and chlorophyll to carotenoids S_1 energy transfer can happen very rapidly on the picosecond and sub-picosecond range (Kloz et al. 2011 and ref. therein). Yet, without precise knowledge of the S_1 state energy of hECN in OCP, the evaluation of its function in PBS quenching as a likely dissipation channel is hardly possible. The S_1 state can be populated after two photon excitation (Holleboom and Walla 2014) or after excitation of the carotenoids in the UV/Visible region to their S_2 state and internal conversion to the S_1 level (Polívka and Sundström 2004). Contemporary spectroscopic technique has allowed recording the optically forbidden $S_1 \rightarrow S_0$ fluorescence emission for carotenoids with such long conjugated chain as $n \geq 11$–13 although the data for highly purified carotenoid samples in organic solvents showed that the $S_1 \rightarrow S_0$ emission yields are almost negligible ($\sim 10^{-6}$) (Fuji et al. 2001; Niedwiedzki et al. 2007). Fluorescence emission of hECN in OCP ($n = 11$) is unknown and its detection seems to be hardly possible because buffer-containing protein solutions cannot be purified so thoroughly as organic solvents. Nevertheless, recently, the S_1 state energy of hECN in OCP has been investigated by time-resolved spectroscopic methods after measuring the spectrum of the $S_1 \rightarrow S_2$ transition in the near IR region and subtracting this energy from that of the $S_0 \rightarrow S_2$ transition obtained from steady-state spectra. It was shown that the S_1 state of hECN (0–0 band) in OCP^o lies at 14,650 cm^{-1} (corresponding to the wavelength of 680 nm) and in OCP^r at 14,025 cm^{-1} (713 nm); these energy values have error bars of 200 cm^{-1} due to the uncertainty in the position of the spectral bands in the amplitude spectra caused the global fitting procedure (Polívka et al. 2013).

Comparison with the fluorescence emission peak position of PBL_{CM} (Fig. 6) showed that it completely coincides with the 0–0 band of hECN S_1 absorption state in OCP^o and slightly differs from corresponding wavelength of OCP^r but although fall into the region of high spectral overlap. Besides, because the OCP absorption is theoretically much broader than the PBL_{CM} emission, the spectral overlap is insensitive to its precise description (Krueger et al. 2001). Complete coincidence of the main peak position in absorption spectrum of the donor with the fluorescence emission spectrum of the acceptor is a sign of their possible excitonic coupling meaning that the carotenoid S_1 excited state has to be in resonance with the S_1 phycobilin excitation. Comparing to the spectral bands overlap, the distance R between the centers of mass of interacting donor and acceptor molecules is important parameter but it does not indicate itself the presence or absence of their excitonic coupling (Agranovich 1982). We define the ground states of the donor and acceptor chromophore molecules wave functions as φ_D and φ_A, as well as excited states φ_D* and φ_A*, correspondingly. Excitonic coupling between the donor and acceptor chromophores becomes possible in case of identity of the energy gap, ΔE, of the ground and excited states for a pair of chromophores, e.g., $\Delta E = E_D^* - E_D^0 = E_A^* - E_A^0$. Under these conditions, the state of the "donor–acceptor" pair system is degenerate and is described by the wave functions $\Psi_1 = \varphi_D{}^*\varphi_A$ and $\Psi_2 = \varphi_D\varphi_A{}^*$. In case of donor–acceptor interaction, the degeneracy is removed and degenerative energy level splits into two sublevels. Between these sublevels the quantum oscillations occur with the frequency that determines the period (characteristic time) of the energy transfer (Agranovich 1982; Egorov and Alfimov 2007). An interaction mechanism periodically de-excites an initially excited electron on the donor molecule and simultaneously excites an initially de-excited electron on the acceptor molecule and vice versa. The total Hamiltonian H for the "donor–acceptor" system in this case can be written as

$$\hat{H} = \hat{H}_D(r_1) + \hat{H}_A(r_2) + \hat{V}(r_1, r_2, R), \tag{10}$$

where $\hat{H}_D$ and $\hat{H}_A$ are the Hamiltonians for the isolated donor and acceptor, respectively, which satisfy two independent Schrödinger equations:

$$\begin{aligned} \hat{H}_D\varphi_D &= E_D\varphi_D \\ \hat{H}_A\varphi_A &= E_A\varphi_A \end{aligned} \tag{11}$$

$\hat{V}$ is the interaction Hamiltonian between the donor and acceptor; R is a vector of the distance between the centers of mass of these molecules mentioned above; r_1 and r_2 are the electronic and nuclear coordinates of the donor and acceptor molecules, correspondingly. States $\Psi_1 = \varphi_D{}^*\varphi_A$ and $\Psi_2 = \varphi_D\varphi_A{}^*$ are the eigen states of the Hamiltonian of the non-interacting chromophores:

$$\hat{H}_0 = \hat{H}_D(r_1) + \hat{H}_A(r_2). \tag{12}$$

Assuming $V \ll |E^* - E^0|$, perturbation theory can be used. Considering the Hamiltonian in the form of Eq. 10, we seek the full solution (Ψ) of the time-dependent Schrödinger equation as a linear expression that includes the phase factor a of the stationary states of the non-perturbed system ($\Psi 1$ and $\Psi 2$)

$$\begin{aligned}\Psi(r,t) = a_1\Psi_1 \exp\left(\frac{-i\,(E^0 - E)\,t}{\hbar}\right)\\ + a_2\Psi_2 \exp\left(\frac{-i\,(E^0 - E)\,t}{\hbar}\right)\end{aligned} \tag{13}$$

Combining Eqs. 10, 11, and 13 and the Schrödinger equation, after reduction, we get a system of equations describing the phase factor behavior:

$$\begin{aligned} i\hbar\dot{a}_1 &= a_2 V_{12}\\ i\hbar\dot{a}_2 &= a_1 V_{21}\end{aligned}, \tag{14}$$

where, under the Dirac notation, $V_{12} = V_{21} = \langle \Psi_2|\hat{V}|\Psi_1\rangle$ is a matrix element determining the probability of a transition from state Ψ_1 to state Ψ_2 and vice versa. The solution of this system gives the characteristic time of energy migration from the donor to the acceptor molecule, τ_m (Egorov and Alfimov 2007). This time is equal to the half-time of the corresponding quantum oscillation period between states Ψ_1 and Ψ_2:

$$\tau_m = \frac{\pi\hbar}{|V_{12}|}. \tag{15}$$

Because the state Ψ_1 to state Ψ_2 transition is realized under condition of the dipole–dipole interaction between donor and acceptor molecules, the matrix element is calculated by integrating

$$|V_{12}| = \frac{\chi\, p_A p_D}{n^3 R^3}, \tag{16}$$

where χ, p_A, p_D, n, and R are the same as in Eq. 1.

Carotenoid hECN has a carbonyl group at one end of the conjugated system and, within OCP, *H*-bonded Tyr-203 and Trp-290 aminoacid residues, strongly influencing the polyene symmetry. Also the symmetry is affected by bending of hECN molecule (Fig. 1e) due to the interaction with surrounding amino acids. The effect of symmetry breaking indicates that the $S_0 \leftrightarrow S_1$ transition dipole moment is distinct from zero but it is too small to be amenable to direct measurement (Ritz et al. 2000). Therefore, we calculated the transition dipole moments both of hECN and phycobilin of PBL_{CM} to analyze possible energy coupling of these chromophores. According to quantum chemical calculations (see "Transition dipole moments calculations" section), the transition dipole moment of the hECN S_1 state has the value of 1.83 D, and, according to normalized fluorescence emission spectrum (see Eq. 9), the transition dipole moment of phycobilin of PBL_{CM} has value of 10.20 D. Both values are in the range of reported for other carotenoids (Krueger et al. 2001; Matamala et al. 2007) and for phycobilin chromophores in PBS (Ren et al. 2013). Putting both values in Eqs. 15 and 16 gives $\tau_m = 36$ ps.

This time makes the mechanism of direct interaction of excited phycobilin of PBL_{CM} with the S_1 state of hECN very competitive compared to mentioned above energy migration to PS II within 200 ps, and therefore, it is very probable in OCP-induced PBS energy quenching. The average lifetime of the PBS, as mentioned above, in the absence of the OCP is $\tau_{PBS} = 1800$ ps. The evaluation of the efficiency η of EET by calculating the ratio of the fluorescence lifetimes of the donor in the absence and the presence of the acceptor gives, according to Förster (1965), the value of $\eta = 1 - \tau_{migr}/\tau_{PBS} = 0.98$. This value is very high, but in the cyanobacterial cell the OCP-induced quenching competes with the time of energy migration from PBS to the reaction centers of $\sim$200 ps (Holzwarth 1992). This process diminishes the efficiency of quenching to $\eta = 1 - \tau_{migr}/\tau_{PBS} = 0.82$. To complete this paragraph, the value of exciton splitting ΔE_{ex} in case of non-zero donor and acceptor transition dipole moments can be represented in a classic form as an energy of dipole–dipole interaction (Agranovich 1982):

$$\Delta E_{ex} = 2|V_{12}|. \tag{17}$$

According to Eqs. 16 and 17, ΔE_{ex} is equal to the very small value of 0.3 cm^{-1} that cannot be resolved in steady-state spectra.

Discussion

Properties of the 3D model of OCP–PBS interaction

In the present work, using computational simulations we arrived at a rational model of the OCP–PBS complex structure that allowed theoretical calculations of energy transfer and quenching. The exact binding site of OCP will remain a subject of discussion until crystal structure data for the PBS core become known. Lack of structural knowledge of OCP^r also prevented its final assignment in

the PBS. It was hypothesized that OCP can bind to any bulk APC_{660} trimers, which implies several nonspecific binding sites per PBS because of the multiple copies of APC_{660} in the PBS core (Kirilovsky and Kerfeld 2013). In contrast to the revealed physical contact of OCP with isolated L_{CM} (Stadnichuk et al. 2012, 2013), this assumption is difficult to combine with current lack of evidence of the interaction between OCP and isolated APC trimers in solution (Stadnichuk et al. 2012). An earlier suggestion that OCP could interact with the PBS only via its *C*-terminal domain (Kirilovsky and Kerfeld 2013) was based on the structural similarity of this domain composed of α-helical and β-sheet motifs and the small $L_{7.8}$ core linker protein present inside the central cavity of APC rods. The model is in contradiction with the constant disposition of $L_{7.8}$ in the external trimers of the APC-built cylinders in the PBS core (Adir 2005; Watanabe and Ikeuchi 2013), which would block the free access of OCP. Based on experiments with mutant cells, this suggestion was reconsidered in favor of the *N*-terminal domain and the assumption that the positively charged Arg155 residue in the *N*-terminal OCP domain is involved in the interaction with PBS (Wilson et al. 2012). Recently, confirmation of the participation of L_{CM} in anchoring the OCP was obtained by mapping of cross-linking species between the OCP and PBS core peptide components. Among the three determined cross-link peptides closely involved in the OCP–PBS association, one contained a lysine that belongs to L_{CM} (Zhang et al. 2014). On the basis of protein cross-linking, the OCP was putted by its *N*-terminal domain between two APC trimers, APC660 and another one, which contains PBL_{CM} (Zhang et al. 2014). In this model one or both neighboring APC-disks in the native structure of PBS should be moved apart. Besides, under this assumption, the closest distance between carotenoid and the nearest phycobilin molecule (25.8 Å, Zhang et al. 2014) is greater than in our model (24.7 Å). Because distance strongly dictates EET efficiency and because APC_{660} cannot gather energy from all other chromophores of PBS like PBL_{CM} does, this hypothesis is not free from shortcomings as well.

Our model has some serial advantages. MD simulations verified the revealed thermodynamic possibility of the proposed geometry of OCP–PBS complex formation. The discerning of PBL_{CM} as the attachment site for OCP between very similar in geometry polypeptide subunits of APC is easily explained by the interaction of OCP with the folded PB loop present in L_{CM}. According to the model, the calculated high effectiveness of quenching corresponds to the determined dipole transition moments of neighboring OCP and PBL_{CM} chromophores and their center-to-center distance. Also, our model of the attachment of OCP to the PBS surface strongly suggests the disruption of the salt bridge between Arg155 and Glu244, which are in the interface between the *N*- and *C*-terminal domains in the central OCP cavity (Kerfeld 2004). Earlier, by site-directed mutagenesis it was demonstrated that the salt bridge between the strongly conserved Arg155 and Glu244 residues in OCP^r, in contrast to OCP^o, is really weaker or nonexistent (Wilson et al. 2012). The important feature of our model is its universality: interdomain OCP cavity participates in forming of attachment sites in OCP–PBL_{CM} and OCP–FRP interactions. Crystallographic and computational experiments would be very useful for improving extant models. The crystallization of the "quenched" OCP^r–PBS complex may provide more detailed information about the site of OCP binding.

Possible OCP-dependent quenching mechanisms

OCP^r induces a decrease in PBS fluorescence by thermal energy dissipation, and, consequently, a decrease in the number of excitations arriving at photosynthetic reaction centers. As far as we know, before this work no theoretical energy transfer rates of the formed OCP–PBS complex have been reported. Although our analysis uses some approximations, it does provide a reasonable calculated value for the time and effectiveness of OCP-dependent NPQ and is consistent with the spectral and geometrical properties of OCP and PBS. The rate constants for quenching in cells and isolated PBS have been investigated by time-resolved spectroscopic methods. In cells, the overall experimental rate constant for quenching was determined as $(16 \pm 4\ \text{ps})^{-1}$ (Tian et al. 2011). Moreover, since only one of the about 70 phycobilin pigment molecules present in the PBS core is directly quenched by the OCP, the rate constant for molecular quenching was proposed to be at most $(240 \pm 60\ \text{fs})^{-1}$, which is extremely fast (Tian et al. 2011). However, this proposal needs to be verified by quantitative analysis of energy transfer pathways among all the chromophores of the three APC cylinders forming the PBS core. Besides, the fluorescence lifetime is a coarse measurement as it is a measure of the sum of all the excitation populations as a function of time and it has been shown that different kinetic models can fit the fluorescence lifetime data equally well (Zaks and Amarnath 2013). Nevertheless, the qualitative agreement between our semiempirical calculations ($36\ \text{ps}^{-1}$) and experimental studies ($16\ \text{ps}^{-1}$) suggests that the method used here is sufficient to depict the EET pathway.

We cannot reveal the precise mechanism of how excitation energy is transferred from the PBL_{CM} to chlorophyll because of the challenge of finding the accurate location of PBL_{CM} in the corresponding APC trimers of the two bottom PBS core cylinders and the unsolved association of PBS to photosystems I and II (Mullineaux 2008). Nevertheless, it is known that EET from the PBS core to

photosystem II is equal to 170–230 ps from the data reported in the literature (Sharkov et al. 1994 and references therein). The rate constant of energy quenching by OCP equal to 36 ps competes well with this data, indicating that proposed mechanism of energy quenching is quite reasonable. Additional ultrafast transient absorption measurements of OCP–PBS complexes will be needed to verify the experimental and theoretical data. The lateral walls of the central cavity in the OCP molecule could be dynamically moved aside when OCP is anchored to the PBS. As a result, the two interacting chromophores could be at the actually shorter distance than the determined 24.7 Å. Nevertheless, our MD simulations have demonstrated that the salt bridge between R155 and E244 aminoacid residues inside the central OCP cavity was flexible but stayed non-disrupted in this process. Therefore, the distance can be shortened unessential, not more then by 0.1–0.3 Å, not influencing sufficiently the time of inter-chromophore energy migration. Besides, the calculated time of migration equal to 36 ps corresponds reasonably well to the obtained experimentally (Tian et al. 2011).

ICT state of OCP

Carbonyl carotenoids characterized like hECN by a keto carbonyl group partially conjugated with the π-system of carbon backbone, possess an intramolecular charge-transfer (ICT) state (Zigmantas et al. 2004). The ICT state is usually strongly coupled to the S_1 state and, in general, the efficiency of energy quenching by carotenoids increases with ICT state formation (Zigmantas et al. 2004). Spectral bands in the transition absorption spectra of OCP-bound hECN demonstrate features typical for the ICT state (Polívka et al. 2005). It was proposed that the S_1 energies of hECN in both OCP^o and OCP^r are low enough to quench the PBS directly by energy transfer (Polívka et al. 2013). While the ICT state exhibits charge-transfer character, it was concluded) that OCP^r may act as a mediator in an intermolecular charge transfer from phycobilins of PBS and fulfill a charge-transfer quenching mechanism (Tian et al. 2011). The separation between the adjacent chromophores of OCP and PBL_{CM} is virtually 25 Å (Fig. 1e), which is too far for effective inter-chromophore charge transfer. Therefore, the question arises about the role of ICT state in OCP.

Activation of the ICT state leads to a shortening of the hECN lifetime and makes the protein-bound hECN a more effective energy dissipater. In the excited state of OCP^r the contribution of the ICT state is larger than in OCP^o (Berera et al. 2012). According to the most recent data (Berera et al. 2013), photoactivated OCP is characterized by one state with predominantly ICT character (ICT/S_1) and a lifetime of 2.3 ps, and another state with mainly S_1 character (S_1/ICT) with a lifetime of 7.6 ps. In peridinin, the ICT state would be expected to yield significantly more dipole strength than the S_1 transition alone (Krueger et al. 2001). Therefore, we suggest that, according to our estimation of the role of the $S_1 \rightarrow S_0$ transition of hECN in direct energy quenching, the importance of OCP^r formation from OCP^o consists in the increase in the ICT state. Clearly, more theoretical and experimental work is needed to sufficiently explain the photophysics of hECN in the photoactive and photoinactive forms of OCP.

Carotenoid-dependent NPQ in cyanobacteria and chloroplasts

For a long time, carotenoid-dependent NPQ has been associated only with chlorophyll-containing antennal complexes of chloroplasts with a conversion of violaxanthin to zeaxanthin as the key reaction initializing this process (for reviews see Ruban et al. 2012 and Ruban et al. 2014). A number of studies in the last decade have shown that a reversible quenching related to carotenoids (hECN) also exists in the PBS antenna of cyanobacteria. It was proposed that the OCP activation could be viewed as a simplified version of the xanthophyll cycle; while the xanthophyll cycle requires interconversion of two different carotenoids, in the OCP the comparable changes of carotenoid absorption properties are achieved via light-induced OCP^o to OCP^r interconversion (Polívka et al. 2013). The precise molecular organization and function of the two NPQ mechanisms is rather different. The average separation of chlorophyll and carotenoid molecules in light-harvesting antennal complexes is within Van der Waals contact (i.e., <3.6 Å) (Stroebel et al. 2003), while hECN of OCP is separated from the chromophore of PBL_{CM} by about 25 Å. In this respect, the OCP is closer to the b_6f-cytochrome complex, where the distance between carotenoid and chlorophyll molecules is equal to 14 Å (Stroebel et al. 2003). Besides, xanthophylls involved in NPQ in plant chloroplasts do not contain carbonyl groups; an ICT state is not formed in these carotenoids, like it is estimated for hECN. The other difference is that xanthophylls are permanently present within the chlorophyll *a/b*-containing antenna, and the availability of high-resolution X-ray structures allows the study of excitation transfer between carotenoids and chlorophylls involved in photoprotection and light harvesting on the basis of a known geometry of the chromophore aggregates (Zaks and Amarnath 2013; Holleboom and Walla 2014). In contrast, the PBS is devoid of intrinsic carotenoids because PBS is a water-soluble complex, and building of the attachment model for OCP and PBS is a prerequisite for subsequent calculations.

Summary model of the NPQ phenomena in antenna of cyanobacteria including OCP, PBS, and FRP interactions

Our working model of OCP-dependent NPQ in cyanobacteria summarizes the data reported here with results of the other authors considering the aggregate state of OCP and FRP in solution and in crystal forms (Kirilovsky and Kerfeld 2013). These data supplement each other and produce an integral landscape of the process (Fig. 7). Under low light or dark conditions, OCP^o in cyanobacteria mainly exist in the form of dimers (Zhang et al. 2014) with surfaces of both OCP monomers that include a central cavity between the *N*- and *C*-domains engaged in OCP^o-dimer formation (Wilson et al. 2008). The existence of OCP^o mainly in the form of dimers is at the bottom why, as is well known, the PBS cannot bind OCP^o. Under high light conditions, the photoprotective cycle starts: OCP^o is converted into OCP^r, which undergoes a conformational change that dissociates the OCP^o dimers to OCP^r monomers (Zhang et al. 2014). After that the monomeric OCP^r anchors to the PBS core to quench excess energy. Like OCP^o, the FRP also exists mainly in dimeric form (Sutter et al. 2013). Co-immunoprecipitation experiments demonstrated that FRP interacts only with OCP^r (Boulay et al. 2010), while the dimers of OCP^o and FRP do not interact with each other because they have no conforming surface areas that can slip together. The aggregation state of FRP could be regulated by exterior factors that reversibly dissociate a protein dimer into monomeric form. Under high light conditions, the increase in OCP^r concentration leads to its partial association with monomeric FRP, which competes with the PBS for binding of OCP^r. The FRP dissociates from the OCP^r–FRP heterodimer after the back transformation of OCP^r into OCP^o. Depending on light and environmental conditions, a dynamic equilibrium is formed between monomeric and dimeric forms of OCP and FRP and quenched and unquenched states of PBS (Fig. 7).

Co-evolutional destiny of OCP and PBS

PBSs were lost during the evolutionary origin of chloroplasts from cyanobacteria in higher plants and most taxa of algae, but there is currently no evidence for genes encoding OCP in the red algae and glaucophytes that have PBSs serving for light harvesting as well (Niyogi and Truong 2013; Watanabe and Ikeuchi 2013). Some extant cyanobacteria despite of the presence of PBSs lack OCP too (Kirilovsky and Kerfeld 2013). Without OCP, the question how these photosynthetic organisms regulate light absorption and energy transfer in the PBS was asked in (Niyogi and Truong 2013). We suppose that OCP

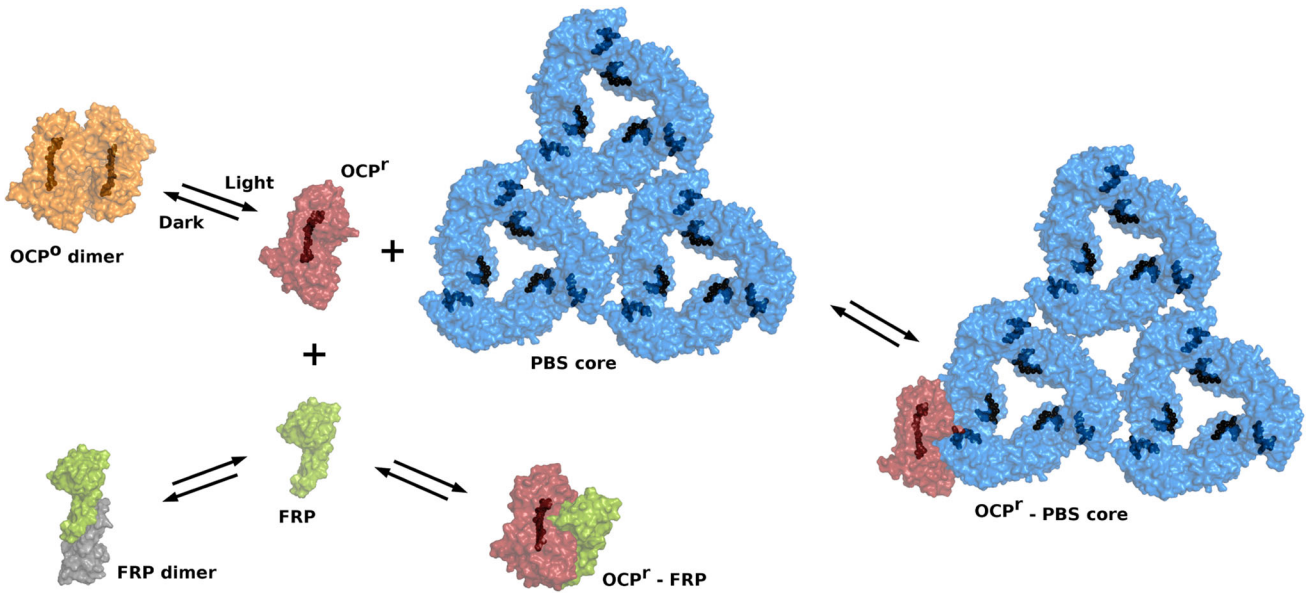

Fig. 7 Model of the interplay between FRP, OCP, and PBS under high light and dark conditions. Under low light or dark conditions, OCP^o and FRP exist in the form of dimers that cannot interact with each other. Under the same conditions, all of the PBS will be free of OCP and unquenched because the OCP^o dimer cannot bind to the PBS. The OCP^o dimer under high light conditions undergoes a conformational change, converts into the OCP^r, and simultaneously dissociates to monomers. OCP^r anchors to the PBS core to quench excess energy. The aggregation state of FRP could be regulated by exterior factors that reversibly dissociate it into a monomeric form. Under high light conditions, the increase in the OCP^r concentration leads to its partial association with monomeric FRP, which concurrently prevents OCP^r attachment to the PBS. FRP dissociates from the OCP^r–FRP heterodimer after the back transformation of OCP^r into OCP^o

disappeared in seaweeds like the red algae and cyanobacterial species that are not exposed to high light or strong light fluctuations in their ecological niches. Besides, according to our model it is not evident how, in macrophytic red algae, the attachment of OCP to the surface of hemiellipsoidal PBS, being two times larger than the hemidiscoidal PBS of cyanobacteria (Adir 2005; Watanabe and Ikeuchi 2013), would be effective in the NPQ process. How excess light is neutralized in PBS- and phycobiliprotein-containing eucaryotic algae (cryptophyte, glaucophyte, and red algae) is not well understood, and this agenda could be a fruitful area for study. In particular, it was demonstrated that in unicellular red algae of the *Galdieria* genus, under high light conditions the PBSs could be reversibly detached from the thylakoid membrane with consequent diminished energy transfer to chlorophyll (Stadnichuk et al. 2011A).

Acknowledgments The authors thank Russian Science Foundation (Project 14-14-00589) for financial support.

References

Adir N (2005) Elucidation of the molecular structures of components of the phycobilisome: reconstructing a giant. Photosynth Res 85:15–32

Agranovich VM, Galanin MD (1982) Electronic excitation energy transfer in condensed matter. North-Holland Publishing Co, Amsterdam

Ajlani G, Vernotte C (1998) Deletion of the PB-loop in the L_{CM} subunit does not affect phycobilisome assembly or energy transfer functions in the cyanobacterium *Synechocystis* sp. PCC 6714. Eur J Biochem 257:154–159

Ajlani G, Vernotte C, DiMagno L (1995) Phycobilisome core mutants of *Synechocystis* PCC 6803. Biochim Biophys Acta 1231:189–196

Arteni AA, Ajlani G, Boekema EJ (2009) Structural organization of phycobilisomes from *Synechocystis* sp. strain PCC 6803 and their interaction with the membrane. Biochim Biophys Acta 1787:272–279

Baker N, Sept D, Joseph S (2001) Electrostatics of nanosystems: application to microtubules and the ribosome. Proc Natl Acad Sci USA 98:10037–10041

Berera R, van Stokkum IHM, Gwizdala M, Wilson A, Kirilovsky D, van Grondelle R (2012) The photophysics of the orange carotenoid protein, a light-powered molecular switch. J Phys Chem B 116:2568–2574

Berera R, Gwizdala M, van Stokkum IHM, Kirilovsky D, van Grondelle R (2013) The excited states of the inactive and active forms of the orange carotenoid protein. J Phys Chem B 117:9121–9128

Bernát G, Schreiber U, Sendtko E, Stadnichuk I, Rexroth S, Rögner M, Koenig F (2011) Unique properties versus common themes: the atypical cyanobacterium *Gloeobacter violaceus* PCC 7421 is capable of state transitions and blue-light-induced fluorescence quenching. Plant Cell Physiol 53:528–542

Boulay C, Wilson A, D'Haene S, Kirilovsky D (2010) Identification of a protein required for recovery of full antenna capacity in OCP-related photoprotective mechanism in cyanobacteria. Proc Natl Acad Sci USA 107:11620–11625

Brejc K, Ficner R, Huber R, Steinbacher S (1995) Isolation, crystallization, crystal structure analysis and refinement of allophycocyanin from the cyanobacterium *Spirulina platensis* at 2.3 Å resolution. J Mol Biol 249:424–440

Breneman M, Wiberg KB (2004) Determining atom-centered monopoles from molecular electrostatic potentials: the need for high sampling density in formamide conformational analysis. J Comp Chem 11:361–373

Capuano V, Braux A-S, Tandeau de Marsac N, Houmard J (1991) The "anchor polypeptide" of cyanobacterial phycobilisomes. Molecular characterization of the *Synechococcus* sp. PCC 6301 *apcE* gene. J Biol Chem 266:7239–7247

Egorov VV, Alfimov MV (2007) Theory of the J-band: from Frenkel exciton to the charge transfer. Phys–Uspekhi 50:985–1029

Förster T (1965) In: Sinanoglou O (ed) Modern quantum chemistry. Academic Press, New York, pp 93–137

Fuji R, Ishikawa T, Koyama Y, Taguchi M, Isobe Y, Nagae H, Watanabe Y (2001) Fluorescence spectroscopy of all-trans-anhydrorhodovibrin and spirilloxanthin: detection of the $1B_u^-$ fluorescence. J Phys Chem A 105:5348–5355

Gall A, Henry S, Takaichi S, Robert B, Cogdell RJ (2005) Preferential incorporation of coloured-carotenoids occurs in the LH2 complexes from non-sulphur purple bacteria under carotenoid-limiting conditions. Photosynth Res 86:25–35

Gao X, Wei T, Zhang N, Xie B, Su H, Zhang X, Chen X, Zhou B, Wang Z, Wu J, Zhang Y (2012) Molecular insights into the terminal energy acceptor in cyanobacterial phycobilisome. Mol Microbiol 85:907–915

Gindt YM, Zhou J, Bryant DA, Sauer K (1994) Spectroscopic studies of phycobilisome subcore preparations lacking key core chromophores: assignment of excited state energies to the L_{CM}, β^{18} and α^{AP-B} chromophores. Biochim Biophys Acta 1186:153–162

Glazer AN (1988) Phycobilisomes. Methods Enzymol 167:304–312

Gottschalk L, Lottspeich F, Scheer H (2008) Reconstitution of allophycocyanin from *Mastigocladus laminosus* with isolated linker polypeptide. Photochem Photobiol 58:761–767

Granovsky AA (2011) Extended multi-configuration quasi-degenerate perturbation theory: The new approach to multi-state multi-reference perturbation theory. J Chem Phys 134:214113

Granovsky AA (2014) Firefly version 8.1.0. http://classic.chem.msu.su/gran/gamess/index.html. Accessed 10 Sep 2014

Gwizdala M, Wilson A, Kirilovsky D (2011) In vitro reconstitution system of the cyanobacterial photoprotective mechanism mediated by the orange carotenoid protein in *Synechocystis* PCC 6803. Plant Cell 23:2631–2643

Gwizdala M, Wilson A, Omairi-Nasser A, Kirilovsky D (2013) Characterization of *Synechocystis* PCC 6803 fluorescence recovery protein involved in photoprotection. Biochim Biophys Acta 1827:348–354

Hess B, Kutzner C, van der Spoel D, Lindhal E (2013) GROMACS 4.5: a high-throughput and highly parallel open source molecular simulation toolkit. Bioinformatics 29:848–854

Holleboom CP, Walla PJ (2014) The back and forth energy transfer between carotenoids and chlorophylls and its role in the regulation of light harvesting. Photosynth Res 119:215–221

Holt TK, Krogmann DW (1981) A carotenoid protein from cyanobacteria. Biochim Biophys Acta 637:408–414

Holzwarth AR (1992) Structure-function relationship and energy transfer in phycobiliprotein antennae. Physiol Plant 83:518–528

Holzwarth AR, Bittersma E, Reuter W, Wehrmeyer W (1990) Studies on chromophore coupling in isolated phycobiliproteins. Biophys J 57:133–145

Jallet D, Gwizdala M, Kirilovsky D (2012) ApcD, ApcF and ApcE are not required for the orange carotenoid protein related phycobilisome fluorescence quenching in the cyanobacterium

Synechocystis PCC 6803. Biochim Biophys Acta 1817:1418–1427

Jorgensen WL, Maxwell DS, Tirado-Rives J (1996) Development and testing of the OPLSA all-atom force field on conformational energetics and properties of organic liquids. J Am Chem Soc 118:11225–11236

Karplus M, Kushick JN (1981) Method for estimating the configurational entropy of macromolecules. Macromolecules 14:325–332

Kerfeld CA (2004) Structure and function of the water-soluble carotenoid-binding proteins in cyanobacteria. Photosynth Res 81:215–225

Kirilovsky D, Kerfeld CA (2013) The orange carotenoid protein: a blue–green light photoactive protein. Photochem Photobiol Sci 12:1135–1143

Kloz M, Pilla S, Kodis G, Gust D, Moore TA, Moore AL, van Grondelle R, Kennis JTM (2011) Carotenoid photoprotection in artificial photosynthetic antennas. J Am Chem Soc 133:7007–7015

Knecht S, Marian CM, Kongsted J, Mennucci B (2013) Statistical physics and computer simulations. J Phys Chem B 117:13808–13815

Kollman PA, Massova I, Reyes C, Kuhn B, Huo S, Chong L, Lee M, Lee T, Duan Y, Wang W, Donini O, Cieplak P, Srinivasan J, Case DA, Cheatham TE (2000) Calculating structures and free energies of complex molecules: combining molecular mechanics and continuum models. Acc Chem Res 33:889–897

Krueger BP, Lampoura SS, van Stokkum IHM, Papagiannakis E, Salvedra JM (2001) Energy transfer in peridinin–chlorophyll-*a* protein from *Amphidinium carterae* studied by polarized transient absorption and target analysis. Biophys J 80:2843–2855

Kuzminov FI, Karapetyan NV, Rakhimberdieva MG, Elanskaya IV, Gorbunov MY, Fadeev VV (2012) Investigation of OCP-triggered dissipation of excitation energy in PSI/PSII-less *Synechocystis* sp. PCC 6803 mutant using non-linear laser fluorimetry. Biochim Biophys Acta 1817:1012–1021

Laikov DN (1997) Fast evaluation of density functional exchange-correlation terms using the expansion of the electron density in auxiliary basis sets. Chem Phys Lett 281:151–156

Lakowicz JR (2006) Principles of fluorescence spectroscopy. Springer, New York

Liao PN, Pillai S, Gust D, Moore TA, Moore AL, Walla PJ (2011) Two-photon study on the electronic interaction between the first excited singlet states in carotenoid-tetrapyrrole dyads. J Phys Chem A 115:4082–4091

Makhatadze GI, Privalov PL (1993) Contribution of hydration to protein folding thermodynamics. II. The entropy and Gibbs energy of hydration. J Mol Biol 232:660–679

Matamala AR, Almonacid DE, Figueroa MF, Martinez-Oyanedel J, Bunster MC (2007) A semiempirical approach to the intra-phycocyanin and inter-phycocyanin fluorescence resonance energy-transfer pathways in phycobilisomes. J Comput Chem 28:1200–1207

McGregor A, Klartag M, David L, Adir N (2008) Allophycocyanin trimer stability and functionality are primarily due to polar enhanced hydrophobicity of the phycocyanobilin binding pocket. J Mol Biol 384:406–421

Mullineaux CW (2008) Phycobilisome-reaction centre interaction in cyanobacteria. Photosynth Res 95:175–182

Niedwiedzki D, Koscielecki JF, Cong H, Sullivan JO, Gibson GN, Bridge RR, Frank HF (2007) Ultrafast dynamics and excited state spectra of open-chain carotenoids at room and low temperatures. J Phys Chem B 111:5984–5998

Niyogi KK, Truong TB (2013) Evolution of flexible non-photochemical quenching mechanisms that regulate light harvesting in oxygenic photosynthesis. Curr Opin Plant Biol 16:307–314

Polívka T, Sundström V (2004) Ultrafast dynamics of carotenoid excited states—from solution to natural and artificial systems. Chem Rev 104:2021–2071

Polívka T, Kerfeld CA, Pascher T, Sundström V (2005) Spectroscopic properties of the carotenoid 3′-hydroxyechinenone in the orange carotenoid protein from the cyanobacterium *Arthrospira maxima*. Biochemistry 44:3994–4003

Polívka T, Chábera P, Kerfeld CA (2013) Carotenoid–protein interaction alters the S1 energy of hydroxyechinenone in the orange carotenoid protein. Biochim Biophys Acta 1827: 248–254

Rakhimberdieva MG, Boichenko VA, Karapetyan NV, Stadnichuk IN (2001) Interaction of phycobilisomes with photosystem II dimers and photosystem I monomers and trimers in the cyanobacterium *Spirulina platensis*. Biochemistry 40:15780–15788

Rakhimberdieva MG, Stadnichuk IN, Elanskaya IV, Karapetyan NV (2004) Carotenoid-induced quenching of the phycobilisome fluorescence in photosystem II-deficient mutant of *Synechocystis* sp. FEBS Lett 574:85–88

Rakhimberdieva MG, Elanskaya IV, Vermaas WFJ, Karapetyan NV (2010) Carotenoid-triggered energy dissipation in phycobilisomes of *Synechocystis* sp. PCC 6803 diverts excitation away from reaction centers of both photosystems. Biochim Biophys Acta 1797:241–249

Ren Y, Chi B, Melhem O, Wei K, Feng L, Li Y, Han X, Li D, Zhang Y, Wan J, Xu X, Yang M (2013) Understanding the electronic energy transfer pathways in the trimeric and hexameric aggregation state of cyanobacterial phycocyanin within the framework of Förster theory. J Comp Chem 34:1005–1012

Ritchie DW, Kozakov D, Vajda S (2008) Accelerating and focusing protein-docking correlations using multi-dimensional rotational FFT generating functions. Bioinformatics 24:1865–1873

Ritz T, Damjanovic A, Schulten K, Zhang J-P, Koyama Y (2000) Efficient light harvesting through carotenoids. Photosynth Res 66:125–144

Ruban AV, Johnson MP, Duffy CDP (2012) The photoprotective molecular switch in the photosystem II antenna. Biochim Biophys Acta 1817:167–181

Ruban AV, Belgio E, Duffy CDP (2014) In: Allakhverdiev SI, Rubin AB, Shuvalov VA (eds) Contemporary problems of photosynthesis. Moscow-Izhevsk: Institute of Computer Science, Moscow-Izhevsk, pp 41–68

Schmidt MW, Baldridge KK, Boatz JA, Elbert ST, Gordon MS, Jensen JH, Koseki S, Matsunaga N, Nguyen KA, Su S, Windus TL, Dupuis M, Montgomery JA (1993) General atomic and molecular electronic structure system. J Comp Chem 14:1347–1363

Scott M, McCollum C, Vasil'ev S, Grozier C, Espie GS, Krol M, Huner NP, Bruce D (2006) Mechanism of the down regulation of photosynthesis by blue light in the cyanobacterium *Synechocystis* sp. PCC 6803. Biochemistry 45:8952–8958

Sharkov A, Kruykov I, Khoroshilov E, Kruykov P, Fisher R, Scheer H (1994) Femtosecond spectral and anisotropy study of excitation-energy transfer between neighbouring alpha-80 and beta-81 chromophores of allophycocyanin trimers. Biochim Biophys Acta-Bioenerg 1188:349–356

Sinanoglou O (1965) Modern quantum chemistry. Academic Press, New York, pp 93–137

Stadnichuk IN, Lukashev EP, Elanskaya IV (2009) Fluorescence changes accompanying short-term light adaptations in photosystem I and photosystem II of the cyanobacterium *Synechocystis* sp. PCC 6803 and phycobiliprotein-impaired mutants: state 1/state 2 transitions and carotenoid-induced quenching of the phycobilisomes. Photosynth Res 99:227–241

Stadnichuk IN, Bulychev AA, Lukashev EP, Sinetova MS, Khristin MS, Johnson MP, Ruban AV (2011a) Far-red light-regulated efficient energy transfer from phycobilisomes to photosystem I in the red microalga *Galdieria sulphuraria* and photosystems-related heterogeneity of phycobilisome population. Biochim Biophys Acta 1807:227–235

Stadnichuk IN, Yanyushin MF, Zhgarmukhamedov SK, Maksimov EG, Muronez EM, Paschenko VZ (2011b) Quenching of phycobilisome fluorescence by orange carotenoid-protein. Doklady Biochem Biophys 439:167–170

Stadnichuk IN, Yanyushin MF, Maksimov EG, Lukashev EP, Zharmukhamedov SK, Elanskaya IV, Paschenko VZ (2012) Site of non-photochemical quenching of the phycobilisome by orange carotenoid protein in the cyanobacterium *Synechocystis* sp. PCC 6803. Biochim Biophys Acta 1817:1436–1445

Stadnichuk IN, Yanyushin MF, Bernát G, Zlenko DV, Krasilnikov PM, Lukashev EP, Maksimov EG, Paschenko VZ (2013) Fluorescence quenching of the phycobilisome terminal emitter L_{CM} from the cyanobacterium *Synechocystis* sp. PCC 6803 detected in vivo and in vitro. J Photochem Photobiol B Biol 125:137–145

Stroebel D, Choquet Y, Popot YL, Picot D (2003) An atypical haem in the cytochrome $b(_6)$f complex. Nature 26:413–418

Sutter M, Wilson A, Leverenz RL, Lopez-Igual R, Thurotte A, Salmeen AE, Kirilovsky D, Kerfeld CA (2013) Crystal structure of the FRP and identification of the active site for modulation of OCP-mediated photoprotection in cyanobacteria. Proc Natl Acad Sci USA 110:10022–10027

Tian L, van Stokkum JHM, Koehorst RBM, Jongerius A, Kirilovsky D, van Amerongen H (2011) Site, rate and mechanism of photoprotective quenching in cyanobacteria. J Am Chem Soc 133:18304–18311

Tian L, Gwizdala M, van Stokkum JHM, Koehorst RBM, van Amerongen H (2012) Picosecond kinetics of light harvesting and photoprotective quenching in wild type and mutant phycobilisomes isolated from the cyanobacterium *Synechocystis* sp. PCC 6803. Biophys J 102:1692–1700

Watanabe M, Ikeuchi M (2013) Phycobilisome: architecture of a light-harvesting supercomplex. Photosynth Res 116:265–276

Wilson A, Ajlani G, Verbavatz J-M, Vass I, Kerfeld CA, Kirilovsky D (2006) A soluble carotenoid protein involved in phycobilisome-related energy dissipation in cyanobacteria. Plant Cell 18:992–1007

Wilson A, Punginelli C, Gall A, Bonetti C, Alexandre M, Routaboul J-M, Kerfeld CA, van Grondelle R, Robert B, Kennis JTM, Kirilovsky D (2008) A photoactive carotenoid protein acting as light intensity sensor. Proc Natl Acad Sci USA 33:12075–12080

Wilson A, Kinney JN, Zwart PH, Punginelli C, Haene SD, Perreau F, Klein MG, Kirilovsky D, Kerfeld CA (2010) Structural determinants underlying photoprotection in the photoactive orange carotenoid protein of cyanobacteria. J Biol Chem 285:18364–18375

Wilson A, Gwizdala M, Mezzettti A, Alexandre M, Kerfeld CA, Kirilovsky D (2012) The essential role of the *N*-terminal domain of the orange carotenoid protein in cyanobacterial photoprotection: importance of a positive charge for phycobilisome binding. Plant Cell 24:1972–1983

Wu YP, Krogmann DW (1997) The orange carotenoid protein of *Synechocystis* PCC 6803. Biochim Biophys Acta 1322:1–7

Zaks J, Amarnath K (2013) Models and measurements of energy-dependent quenching. Photosynth Res 116:389–409

Zhang H, Liu H, Niedzwiedzki DM, Prado M, Jiang J, Gross ML, Blankenship RE (2014) Molecular mechanism of photoactivation and structural location of the cyanobacterial orange carotenoid protein. Biochemistry 53:13–19

Zhao K-H, Su P, Böhm S, Song B, Zhou Mbubenzer C, Scheer H (2005) Reconstitution of phycobilisome core-membrane linker, L_{CM}, by autocatalytic chromophore binding to ApcE. Biochim Biophys Acta 1706:81–87

Zigmantas D, Hiller RG, Sharples FP, Frank HA, Sundström V, Polivka T (2004) Effect of a conjugated carbonyl group on the photophysical properties of carotenoids. Phys Chem Chem Phys 6:3009–3016